Check for updates

New Phytologist

Research

Time-integrated δ^2H in *n*-alkanes and carbohydrates from boreal needles reveal intra-annual physiological and environmental signals

Charlotte Angove[1,2], Guido L. B. Wiesenberg[3], Marco M. Lehmann[4], Matthias Saurer[4], Yu Tang[5], Elina Sahlstedt[1], Tatjana C. Speckert[3], Pauliina P. Schiestl-Aalto[6] and Katja T. Rinne-Garmston[1]

[1]Stable Isotope Laboratory of Luke (SILL), Natural Resources Institute Finland (Luke), Helsinki, 00790, Finland; [2]University of Helsinki, Helsinki, 00790, Finland; [3]Department of Geography, University of Zürich, Zürich, 8057, Switzerland; [4]Forest Soils and Biogeochemistry, Swiss Federal Institute for Forest, Snow and Landscape Research (WSL), Birmensdorf, 8903, Switzerland; [5]College of Urban and Environmental Sciences, Peking University, Beijing, 100871, China; [6]Faculty of Science, Institute for Atmospheric and Earth System Research (INAR)/Physics, University of Helsinki, Helsinki, 00014, Finland

Author for correspondence:
Charlotte Angove
Email: charlotte.angove@helsinki.fi

Received: *5 August 2024*
Accepted: *19 December 2024*

New Phytologist (2025)
doi: 10.1111/nph.20448

Key words: bioindicators, deuterium, forest, isotopes, leaf sugar, leaf water evaporative enrichment, lipids, paleohydrology.

Summary

- Reliable insights from key δ^2H bioindicators, *n*-alkanes and carbohydrates, are hindered by our limited understanding of isotope fractionation processes related to leaf water and primary assimilates. We addressed this with the first study to investigate time-integrated intra-annual δ^2H signals of *n*-alkanes and carbohydrates in a natural forest.
- We sampled 1-yr-old needles (1N) and current-year needles (0N) from five Scots Pine trees in a coniferous forest in Hyytiälä, Finland, biweekly during 2019. The δ^2H of their *n*-alkanes (δ^2H_{alkane}), water-soluble carbohydrates (δ^2H_{WSC}) and starch (δ^2H_{starch}) were evaluated for time-integrated physiological (gas-exchange) and environmental (hydrological) signals.
- Time integration was critical for interpreting δ^2H_{WSC} and δ^2H_{alkane}. Time-integrated net assimilation rate (T:A_n), the strongest signal in δ^2H_{WSC}, correlated negatively with 1N δ^2H_{WSC} (early season) and positively with 0N δ^2H_{WSC} (late season). Unexpectedly, δ^2H_{alkane} exhibited stronger environmental signals in 1N than in 0N, with the most pronounced being physiologically mediated hydrological signals.
- T:A_n is a major signal in intra-annual δ^2H_{WSC} in a boreal forest, subject to seasonal interactions with needle age and δ^2H_{starch}. There could be enough *de novo* *n*-alkane synthesis *in situ* to enhance the reliability of δ^2H_{alkane} as a hydrological indicator, bringing promise to interpretations of the *n*-alkane palaeohydrological record.

Introduction

The stable H isotope ratio (δ^2H) in plant-derived biomarkers (e.g. *n*-alkanes, tree-ring cellulose) has proven value, and profound potential, for insights into paleoenvironmental reconstructions and plant stress response (Dawson *et al.*, 2004; Kahmen *et al.*, 2013; Lehmann *et al.*, 2024a). A key barrier that limits their reliability and implementation is that their H isotope composition can be affected by multiple isotope fractionating (Zhu *et al.*, 2020; Holloway-Phillips *et al.*, 2022; Baan *et al.*, 2023a) and nonfractionating (i.e., mixing; Liu *et al.*, 2021) processes. This can interfere with meaningful environmental or physiological insights from δ^2H values in plant bioindicators (Baan *et al.*, 2023b). Undoubtedly, they will benefit from a thorough examination of how the δ^2H of plant compounds correlates with environmental and physiological signals under natural conditions.

Background

n-Alkanes with chain lengths of 25–35 carbons are straight-chained hydrocarbons found in leaf epicuticular waxes, which can be key contributors to the δ^2H of *n*-alkanes (δ^2H_{alkane}, Table 1) in soils, used to interpret past climate (Dawson *et al.*, 2004; Schefuß *et al.*, 2005; Thomas *et al.*, 2021). Overall, δ^2H_{alkane} acts as an indicator of δ^2H in precipitation (δ^2H_{precip}), modified by leaf evaporative enrichment, local meteorological factors (i.e. evapotranspiration (ET) and relative humidity (RH)) and source water (Sachse *et al.*, 2006), which is further modified by biochemical isotope fractionation (Newberry *et al.*, 2015; Baan *et al.*, 2023a,b). δ^2H_{alkane} in leaves can be related to δ^2H in leaf water ($\delta^2H_{l\text{-}water}$; Freimuth *et al.*, 2017; Zhu *et al.*, 2020; Lehmann *et al.*, 2024b), though not necessarily (McInerney *et al.*, 2011), and evidence from seasonal δ^2H_{alkane} variability of new needles in a natural forest shows that the $\delta^2H_{l\text{-}water}$ signal

© 2025 The Author(s).
New Phytologist © 2025 New Phytologist Foundation.
This is an open access article under the terms of the Creative Commons Attribution License, which permits use, distribution and reproduction in any medium, provided the original work is properly cited.

Table 1 Abbreviations and symbols used in the text.

Abbreviation	Description
NADPH	Nicotinamide adenine dinucleotide phosphate
NSC	Nonstructural carbohydrates
WSC	Water-soluble carbohydrates
δ^2H	Isotope ratio of ^2H compared to ^1H, relative to VSMOW (‰)
δ^2H_{alkane}	δ^2H of *n*-alkanes
δ^2H_{precip}	δ^2H of precipitation
$\delta^2H_{l\text{-}water}$	δ^2H of leaf water
$\delta^2H_{n\text{-}water}$	δ^2H of needle water
δ^2H_{starch}	δ^2H of starch
δ^2H_{WSC}	δ^2H of water-soluble carbohydrates
δ^2H_{source}	δ^2H of source water
δ^2H_{vapor}	δ^2H of water vapor
$\delta^{18}O$	Isotope ratio of ^{18}O compared to ^{16}O, relative to VSMOW (‰)
$\Delta^2H_{n\text{-}water}$	Needle water ^2H enrichment above source (twig) water (‰)
ε_{bio}	Hydrogen isotope offset between *n*-alkanes and leaf water
RH	Atmospheric relative humidity
E	Transpiration rate
A_n	Net assimilation rate
g_s	Stomatal conductance
T:RH	Time-integrated atmospheric relative humidity
T:*E*	Time-integrated transpiration rate
$T{:}A_n$	Time-integrated net assimilation rate
$T{:}g_s$	Time-integrated stomatal conductance
$T{:}\delta^2H_{n\text{-}water}$	Time-integrated δ^2H of needle water
$T{:}\Delta^2H_{n\text{-}water}$	Time-integrated needle water ^2H enrichment above source (twig) water
$T{:}\delta^2H_{source}$	Time-integrated δ^2H of source water
0N	Current-year needles
1N	One-year-old needles
R^2(M)	Marginal R^2. A pseudo-R^2 estimate for the models being tested
R^2(C)	Conditional R^2. A pseudo-R^2 estimate for the models being tested combined with model random effects, such as sampling date, time and site.
ICC	Intraclass correlation. The probability that two values from the same sampling date, and/or tree identity, correlate, on a scale of 0–1.

can be obscured, potentially by changes in carbohydrate sourcing throughout the season (Newberry *et al.*, 2015). Furthermore, the δ^2H_{alkane} in new leaf tissue can record a shift from heterotrophy to autotrophy (Tipple & Ehleringer, 2018), and if leaves are sampled before autotrophy has been fully established, then the $\delta^2H_{l\text{-}water}$ signal may be obscured (Zhu *et al.*, 2020).

Interspecies differences in leaf δ^2H_{alkane} are more constant between 2 yr than for leaf cellulose δ^2H, suggesting that species differences in biosynthetic fractionation for δ^2H_{alkane} are likely the more invariable and less sensitive to environmental variability (Baan *et al.*, 2023a). Meanwhile, at the scale of intraleaf variability, δ^2H_{alkane} is likely more environmentally sensitive than leaf cellulose δ^2H, owing to a higher proportion of autotrophic production during *n*-alkane syntheses (Zhu *et al.*, 2020). Leaf nonstructural carbohydrates, such as sugars (e.g. sucrose and glucose) and starch, are key intermediaries in the transfer of the δ^2H signal from leaf water to cellulose (Holloway-Phillips *et al.*, 2022; Lehmann *et al.*, 2022), as observed for carbon-13 ($\delta^{13}C$) and oxygen-18 ($\delta^{18}O$) (Gessler *et al.*, 2009). It is valuable to understand their role as δ^2H intermediaries between leaf water and tree rings because tree-ring δ^2H can correlate with $\delta^2H_{l\text{-}water}$ (Lehmann *et al.*, 2024a). Yet, prevailing intra-annual physiological or climatic signals from δ^2H_{WSC} and δ^2H_{starch} has not yet been explored in a natural forest. Evidence from a ^2H-enrichment study shows that the δ^2H in leaf sucrose is likely determined by physiological processes (Augusti *et al.*, 2006). Further evidence shows the ^2H offset between leaf sucrose and water having a variable relationship with $\delta^2H_{l\text{-}water}$, in addition to weak relationships with dark respiration, sugar pool turnover time and the proportion of sugar in the sugar and starch pool (Holloway-Phillips *et al.*, 2022). These trends were reinforced by results from the δ^2H of water-soluble carbohydrates (WSCs), a mixture of sugars and sugar alcohols, suggesting that δ^2H in leaf sugars is determined by the relative concentrations of sugars and starch, and leaf gas exchange (Lehmann *et al.*, 2024b). It is thus valuable to observe whether these signals exhibited in glasshouse experiments (Holloway-Phillips *et al.*, 2022; Lehmann *et al.*, 2024b) can also be observed in intra-annual variation of a natural forest. Water-soluble carbohydrates are used as a proxy for leaf sugars (Leppä *et al.*, 2022; Tang *et al.*, 2022; Lehmann *et al.*, 2024b), as the simplest bulk matter extract that can be measured without using compound-specific isotope analysis. We hereafter use leaf WSC δ^2H (δ^2H_{WSC}) as a proxy for leaf sugar δ^2H. This comes at the disadvantage of measuring a diverse group of leaf compounds with different metabolic history.

Even though leaf carbon partitioning between sucrose and starch is likely instrumental to δ^2H in sugars and tree-ring cellulose (Holloway-Phillips *et al.*, 2022; Wieloch *et al.*, 2022; Lehmann *et al.*, 2024a), the δ^2H of starch (δ^2H_{starch}) has not been compared with physiological or environmental trends. δ^2H_{starch} is distinctly different from δ^2H of sugars (Schleucher *et al.*, 1999); therefore, it is important to investigate whether δ^2H_{starch} has different physiological or climatic trends compared with δ^2H in sugars because the temporally variable interaction between the starch and sugar pool may introduce mixed physiological or environmental signals absent from freshly assimilated sugars.

Hydrogen atoms in leaf carbohydrates (e.g. sugars and starch) and *n*-alkanes are derived from the same leaf's water, but their δ^2H are different, owing to their distinct biochemical pathways (Schleucher *et al.*, 1999). For example, among the prominent hydrogen isotope-fractionating processes that can lead to their different δ^2H (Lehmann *et al.*, 2024b), they can source different amounts of H atoms from nicotinamide adenine dinucleotide phosphate (NADPH), and these H atoms from NADPH can be a product of different NADPH-synthesis pathways (Sessions *et al.*, 1999; Zhou *et al.*, 2016; Wijker *et al.*, 2019). Furthermore, their precursor molecule sources can vary between photosynthetic and glycolytic origins and differently represent short-term and long-term storage (Cormier *et al.*, 2018; Zhu *et al.*, 2020; Lehmann *et al.*, 2024b). Further, nonfractionating (i.e., mixing) processes likely further affect carbohydrate and *n*-alkane δ^2H differently, owing to their different metabolic fates – and these are particularly relevant in field studies (e.g. Leppä *et al.*, 2022).

© 2025 The Author(s).
New Phytologist © 2025 New Phytologist Foundation.

14698137, 0, Downloaded from https://nph.onlinelibrary.wiley.com/doi/10.1111/nph.20448 by Luonnonvarakeskus, Wiley Online Library on [24/02/2025]. See the Terms and Conditions (https://onlinelibrary.wiley.com/terms-and-conditions) on Wiley Online Library for rules of use; OA articles are governed by the applicable Creative Commons License

14698137, 0, Downloaded from https://nph.onlinelibrary.wiley.com/doi/10.1111/nph.20448 by Luonnonvarakeskus, Wiley Online Library on [24/02/2025]. See the Terms and Conditions (https://onlinelibrary.wiley.com/terms-and-conditions) on Wiley Online Library for rules of use; OA articles are governed by the applicable Creative Commons License

The combined consequences of isotope-fractionating and non-fractionating processes, to δ^2H_{alkane} and leaf carbohydrate δ^2H, are poorly understood. Therefore, it is highly valuable to investigate δ^2H_{alkane} and leaf carbohydrate δ^2H together, to elucidate their physiological and environmental information, enhancing our understanding of the relative importance of their different drivers.

Temporal integration perspectives

A key step towards elucidating intra-annual physiological and environmental signals from leaf δ^2H_{alkane}, δ^2H_{WSC} and δ^2H_{starch} *in situ* is quantifying important temporal aspects that could otherwise interfere with finding prevailing trends. Time integration has been long-established in the interpretation of $\delta^{18}O$ in organic compounds, especially tree rings (Gessler *et al.*, 2009; Pérez-de-Lis *et al.*, 2022), and it is known to be important for the transfer of the $\delta^{18}O$ signal from leaf water to foliar water-soluble organic matter (Barnard *et al.*, 2007), WSC (Leppä *et al.*, 2022) and resin (Tang *et al.*, 2024). Therefore, it is long overdue to determine whether time-integrated, intraseasonal signals are revealed from δ^2H_{alkane}, δ^2H_{WSC} and δ^2H_{starch}. This is outstandingly relevant for δ^2H_{alkane} because *n*-alkanes are gradually accumulated during leaf development (Jetter *et al.*, 2000). Indeed, leaf wax measurements from the evergreen shrub *Prunus laurocerasus* have shown that the leaf wax layer continues to thicken after leaf expansion; there were 10 molecular layers in 10-d-old leaves during expansion, *c.* 20 molecular layers after 50 d, and 1-yr-old leaves had 35–45 layers (Jetter *et al.*, 2000; Jetter & Schäffer, 2001). Given that new leaf tissue growth coincides with the predominant wax production, it is a reasonable assumption that the leaf δ^2H_{alkane} largely represents only the early stages of the leaf lifespan (Kahmen *et al.*, 2011; Sachse *et al.*, 2015; Freimuth *et al.*, 2017). Other recent studies argue for the continuous formation of *n*-alkanes in leaves during the growing season (Speckert *et al.*, 2023) and rapid response of *n*-alkane formation as a response to environmental stress such as drought, without increased concentration of *n*-alkanes in the wax layer (Srivastava & Wiesenberg, 2018). Since temperature and elevated CO_2 can affect the composition of *n*-alkanes and their precursors, fatty acids, within leaves (Ofiti *et al.*, 2023), the hydrological signal in δ^2H_{alkane} may not only be obscured by integration time but also the variability in conditions exposed to leaves during their integration.

Evidence from WSC $\delta^{18}O$ would suggest that the δ^2H_{WSC} integration period during a growing season can vary from within 48 h to more than 5 d (Leppä *et al.*, 2022). Meanwhile, the δ^2H_{starch} integration period could depend on the relative contribution of transitory starch to the total leaf starch pool. If the leaf starch pool is mostly transitory, the δ^2H_{starch} integration period will likely be 1 d (Weise *et al.*, 2011; Fernandez *et al.*, 2017).

Spatiotemporal integration perspectives

$\delta^2H_{l\text{-}water}$ becomes higher with increased proximity to evaporative sites (Luo & Sternberg, 1992; Gan *et al.*, 2002; Farquhar & Gan, 2003). This phenomenon has demonstrated relevance for leaf spatial patterns in δ^2H of cellulose and δ^2H_{alkane} (Zhu *et al.*, 2020; Liu *et al.*, 2021). Since photosynthetic tissue water can be more exposed to evaporative ^2H enrichment than bulk $\delta^2H_{l\text{-}water}$, leaf water isotope heterogeneity could be relevant for leaf δ^2H_{WSC}, δ^2H_{starch} and δ^2H_{alkane}, like it has been reported for $\delta^{18}O$ in sucrose (Baca Cabrera *et al.*, 2023). Its role could be profound because the δ^2H of source water (δ^2H_{source}) and evaporative ^2H enrichment that make up $\delta^2H_{l\text{-}water}$ are distinctly different (Cernusak *et al.*, 2016); therefore, an increased ratio of evaporative ^2H enrichment could substantially change the δ^2H of surrounding water during *n*-alkane and carbohydrate syntheses. Resultantly, it is not clear whether the long-term δ^2H_{WSC}, δ^2H_{starch} and δ^2H_{alkane} signals are more reflective of needle water δ^2H ($\delta^2H_{n\text{-}water}$) or the ^2H enrichment of needle water above source water ($\Delta^2H_{n\text{-}water}$). Investigating the relative contributions of $\delta^2H_{n\text{-}water}$ and $\Delta^2H_{n\text{-}water}$ to δ^2H_{WSC}, δ^2H_{starch} and δ^2H_{alkane} in natural environments is crucial because it determines the ecohydrological conditions that they represent during palaeohydrological reconstructions.

Study aim and hypotheses

We investigated whether there are time-integrated, physiological or environmental signals in the variability of δ^2H_{alkane}, δ^2H_{WSC} and δ^2H_{starch} using a comprehensive seasonal field survey of *Pinus sylvestris* L. (Scots Pine). We hypothesized that (1) δ^2H_{alkane} and δ^2H_{WSC} have stronger relationships to physiological (leaf gas exchange) or environmental factors (e.g. RH and modeled water isotopes) after accounting for multiple integration days or weeks, and (2) δ^2H_{alkane}, δ^2H_{WSC} and δ^2H_{starch} are more strongly related to time-integrated $\Delta^2H_{n\text{-}water}$ than $\delta^2H_{n\text{-}water}$ because they can be sensitive to inhomogeneities in leaf water (Zhu *et al.*, 2020; Liu *et al.*, 2021), and photosynthetic tissue water is likely more exposed to evaporative enrichment than bulk leaf water (Baca Cabrera *et al.*, 2023). Finally, we hypothesized that (3) based on evidence that δ^2H_{alkane} is related to $\delta^2H_{l\text{-}water}$ in controlled conditions (Freimuth *et al.*, 2017; Lehmann *et al.*, 2024b), enhanced by high autotrophic production in the field (Zhu *et al.*, 2020), δ^2H_{alkane} will reflect $\delta^2H_{l\text{-}water}$ while δ^2H_{WSC} and δ^2H_{starch} will represent leaf gas exchange (Holloway-Phillips *et al.*, 2022; Lehmann *et al.*, 2024b).

Materials and Methods

Field site and sampling procedure

The study site, Hyytiälä Forest (61°51′N, 24°17′E), is a managed forest in central Finland, within the southern boreal vegetation zone. It is dominated by Scots pine (*Pinus sylvestris* L.), 56 yr old during sampling, and other species included Norway spruce (*Picea abies* (L.) H. Karst), birch (*Betula pendula* Roth, *Betula pubescens* Ehrh) and European aspen (*Populus tremula* L.) (Kolari *et al.*, 2022). In 2018, there were 1304 trees ha^{-1}, and the mean tree height was 19.9 m, with dominant tree height reaching 23.5 m (Kolari *et al.*, 2022). The soil, which is a Haplic Podzol, is predominantly < 1 m deep, but there are moist depressions with a thicker layer of soil topped by a thin layer of peat (Kolari *et al.*, 2022). Hyytiälä is part of the Integrated Carbon

© 2025 The Author(s).
New Phytologist © 2025 New Phytologist Foundation.

14698137, 0, Downloaded from https://nph.onlinelibrary.wiley.com/doi/10.1111/nph.20448 by Luonnonvarakeskus, Wiley Online Library on [24/02/2025]. See the Terms and Conditions (https://onlinelibrary.wiley.com/terms-and-conditions) on Wiley Online Library for rules of use; OA articles are governed by the applicable Creative Commons License

Observation System (ICOS) network, and it is a Station for Measuring Forest Ecosystem–Atmosphere Relations (SMEAR). Five Scots pine trees were sampled approximately once every 2 wk over 6 months of 2019, and current-year needle (0N) sampling started when the sample size was large enough, from 12 June 2019 until 11 October 2019. We selected 1N sampling between 30/04 and 08/08, which gave more seasonal coverage of the growing season before 0N were large enough for sampling, and it allowed a 4-wk sampling overlap for 0N and 1N. All needles were collected from sun-exposed branches at 18 m tree height, between 13 and 16 h, and they were immediately transferred to paper bags in a cool box. They were promptly microwaved at 600 W for 1 min to stop enzymatic and metabolic activities (Wanek *et al.*, 2001), and then oven-dried for 24 h at 60°C. Needle samples were homogenized into a fine powder using FastPrep-24™ (MP Biomedicals, Solon, OH, USA).

Extraction and δ^2H analysis of *n*-alkanes

Long-chain leaf wax *n*-alkanes that are frequently used for palaeohydrological reconstructions (Liu *et al.*, 2022) were extracted according to Wiesenberg & Gocke (2015). Homogenized needle material (0.3–1.5 g) was extracted using Soxhlet extraction with a mixture of dichloromethane : methanol (93 : 7; v/v). The extract weights were used to calculate the concentration of total lipid extracts (TLE). Extracts were then sequentially separated by solid phase extraction using KOH (5%)-coated silica gel (SiO_2, 60 Å) into neutral lipid-, fatty acid- and polar lipid fractions. The *n*-alkanes were separated from the neutral lipid fraction using solid phase extraction with activated SiO_2 (100 Å, 110°C overnight). Squalene was added as an internal standard to the *n*-alkane fraction before gas chromatographic (GC) analysis.

n-Alkanes were identified using an Agilent (Santa Clara, CA, USA) 6890N GC equipped with a split/splitless injector coupled to an Agilent 5973 mass selective (MS) detector and external standards and quantified on a GC (Agilent 7890B) equipped with a multimode inlet (MMI) and flame ionization detector. Compound identification of *n*-alkanes was performed using NIST/Wiley spectral libraries and comparison of retention times and mass spectra to external standards (Supelco 68281 with C_{10}–C_{40} *n*-alkanes). Both GC instruments were equipped with a J&W DB-5MS narrow-bore capillary column (50 m × 0.2 mm, 0.33 µm film thickness) and a deactivated precolumn (1.5 m). Helium was used as the carrier gas. The GC oven temperature increased from 70°C (held for 4 min) to 320°C (held for 20 min) at a rate of 5°C min^{-1}. The MMI was kept at 80°C for 0.5 min, ramped to 450°C at a rate of 800°C min^{-1} (held for 2 min) and cooled to 250°C until the end of the oven program.

The *n*-alkane hydrogen isotope composition was determined using a Thermo Fisher Scientific (Waltham, MA, USA) Trace 1320 GC equipped with an split/splitless (S/SL) injector connected via GC-IsoLink II to a ConFlo IV and Delta V Plus isotope mass spectrometer (irMS). Injection was performed, in splitless mode, using an robotic sample handling (RSH) automated liquid sample handling tool using 1–3 µl with a 10-µl syringe at least in triplicate, and in the case of low concentrations or too high deviation between replicates, even more often. For samples with very low alkane abundances, manual injections were performed, if necessary. The temperature of the S/SL injector was 280°C. The capillary column setup and the oven temperature program were identical to the oven temperature program used for quantification. All measurements were performed at least in triplicate. Calibration of δ^2H_{alkane} values was done against A7 and B5 *n*-alkane standard mixtures provided by the Schimmelmann Research laboratory (https://hcnisotopes.earth.indiana.edu/reference-materials/materials-descriptions/n-alkanes.html, accessed 4 May 2024). Regular measurements of secondary standard mixtures (with *n*-C_{20}, *n*-C_{24}, *n*-C_{30}, *n*-C_{32} alkanes) enabled determination of instrument performance and recalibration, if necessary. The precision of δ^2H values of the standard mixtures was better than 1‰ for the individual compounds. If the measured values were outside this range, a reconditioning of the reactor or a recalibration was performed. The measurements of individual samples were run at least in triplicate and only accepted, if the precision of δ^2H values was better than 2‰ for individual compounds. Otherwise, additional replicate measurements were conducted, or further measures were taken, such as adjustment of concentrations to receive satisfying results. The reported δ^2H_{alkane} is provided as the weighted average of the most abundant *n*-alkanes (*n*-C_{25}, *n*-C_{27}, and *n*-C_{29}).

Extraction and δ^2H analysis of WSC and starch

Water-soluble carbohydrates were extracted from needle powder using the hot water extraction method, following the extraction procedure outlined by Wanek *et al.* (2001) and the purification procedure outlined by Rinne *et al.* (2012). Needle starch was extracted from the remaining pellet by enzymatic hydrolysis, according to Wanek *et al.* (2001) and Lehmann *et al.* (2019). These procedures are the same as those in Tang *et al.* (2023) (Supporting Information Methods S1).

Isotope analysis of WSC and starch followed Schuler *et al.* (2022). Samples were double packed into 5.5 × 9 mm silver foil capsules in duplicates. They were then offline equilibrated for 2 h then dried for a further 2 h in N_2 gas, at 130°C (Schuler *et al.*, 2022). Immediately afterwards, samples were transferred to a high-temperature elemental analyzer system coupled to a Delta^{Plus} XP IRMS (Finnigan, Thermo Fisher Scientific) for $^2H/^1H$ measurement. Each sample was analyzed twice, and each round of analysis had an isotopically distinct water for the equilibration. The results typically show that 34–38% of H in sugars is exchangeable, depending on the type of sugar (Schuler *et al.*, 2022). This was considered in the calculation for the nonexchangeable hydrogen isotope ratio (eqn 3 in Schuler *et al.*, 2022). Results were normalized with in-house sugar standards to the Vienna Standard Mean Ocean Water scale. For starch samples, 3 1N sampling days (in May) and 1 0N sampling day were estimated with only one isotopically distinct water; however, their data were included because their variability did not supersede overall seasonal trends, which were confirmed to have not been affected by small sample size. We corrected δ^2H_{starch} and starch concentrations for α-amylase by its relative weight in samples and its measured δ^2H, which had a negligible (< 5‰) influence to 1N δ^2H_{starch} and a relatively low maximum

© 2025 The Author(s).
New Phytologist © 2025 New Phytologist Foundation.

14698137, 0, Downloaded from https://nph.onlinelibrary.wiley.com/doi/10.1111/nph.20448 by Luonnonvarakeskus, Wiley Online Library on [24/02/2025]. See the Terms and Conditions (https://onlinelibrary.wiley.com/terms-and-conditions) on Wiley Online Library for rules of use; OA articles are governed by the applicable Creative Commons License

Table 2 Independent factors selected for comparison to nonstructural carbohydrate δ^2H and *n*-alkane δ^2H, in needles.

Factor	Definition	Reason
RH	Atmospheric relative humidity (%)	Related to leaf water δ^2H and $\delta^{18}O$ (Cernusak *et al*., 2016)
E	Transpiration rate (mol m^{-2} s^{-1})	Relates to leaf water δ^2H and $\delta^{18}O$ via the Péclet effective path length (Song *et al*., 2013). The usefulness of the Péclet correction for tree-ring $\delta^{18}O$ is under question (Ogée *et al*., 2009; Barbour *et al*., 2024); thus, it is valuable to examine for carbohydrate δ^2H
A_n	Net assimilation rate, represented by net CO_2 influx (μmol m^{-2} s^{-1}) measured by cuvette gas exchange, when influx measurements > 0.1 μg m^{-2} s^{-1}	Represents assimilation rate and thus autotrophic status (Yakir, 1992). Related to the hydrogen isotope offset between WSC and water in a controlled experiment (Lehmann *et al*., 2024a).
g_s	Stomatal conductance (mol m^{-2} s^{-1})	Related to photosynthetic activity (Wong *et al*., 1979) and used to model $\delta^2H_{n\text{-}water}$ (e.g. Cernusak *et al*., 2022). Observed relationship to the hydrogen isotope offset between WSC and water in a controlled experiment (Lehmann *et al*., 2024a).
$\delta^2H_{n\text{-}water}$	Modeled bulk needle water ^2H ratio to ^1H. Values relative to VSMOW.	A source of ^2H to *n*-alkanes and carbohydrates (Cormier *et al*., 2018), and *n*-alkanes are hypothesized to represent $\delta^2H_{n\text{-}water}$ (Tipple *et al*., 2015; Zech *et al*., 2015; Hepp *et al*., 2021)
$\Delta^2H_{n\text{-}water}$	Modeled needle water ^2H enrichment above modeled source water	Represents variability of water more exposed to $\Delta^2H_{n\text{-}water}$, which could be more representative of photosynthetic water by leaf water heterogeneity (Liu *et al*., 2021; Baca Cabrera *et al*., 2023)
δ^2H_{source}	Modeled source water ^2H ratio to ^1H. Values relative to VSMOW.	Interpreted from *n*-alkane δ^2H in palaeohydrological studies (Freimuth *et al*., 2017)

VSMOW, Vienna Standard Mean Ocean Water; WSC, water-soluble carbohydrates.

influence (< 13‰) to 0N δ^2H_{starch} considering that the 0N δ^2H_{starch} range was 100‰.

Independent variables for time-integrated comparisons to δ^2H in organic compounds

Our selection of independent variables included a suite of environmental and physiological variables (Table 2). We downloaded RH, transpiration (E), net CO_2 influx (A_n), air temperature and air pressure data from the Smart SMEAR AVAA portal (Aalto *et al*., 2023), at half-hourly resolution. RH was measured onsite by a Rotronic MP102H RH/T sensor at 16.8 m. E and A_n were measured using two automated, box-shaped shoot chamber systems made of acrylic plastic (2.1 dm^3), surrounding debudded shoots in the uppermost canopy (20 m; Aalto *et al*., 2014). Cuvettes were ventilated and equipped with a fan. E was calculated by applying a nonlinear equation to chamber H_2O vapor concentrations during the first 5–35 s of intermittent chamber closures (Kolari *et al*., 2012), while A_n was represented by net needle CO_2 influx, filtered to only include measurements above 0.1 μg m^{-2} s^{-1} to reduce bias from instrument error. When there were missing E or A_n data, we gap filled measurements by implementing the photosynthesis model by Leppä *et al*. (2022), which was parameterized to one of the cuvettes at the study site and represented the chamber's 2019 measurements well ($R^2 = 0.86$, RMSE = 0.04; Fig. S1 inset). We then calculated total leaf conductance to water vapor (g_t; mol m^{-2} s^{-1}) from E (mol m^{-2} s^{-1}) using the following equation:

$$g_t = \frac{E \times (p - \dot{e})}{(e_i - e_a)}$$

where p is air pressure (kPa), e_i is leaf intercellular vapor pressure (kPa), which we assumed to be saturated for the coarse-scale implementation of g_t in this study, e_a is atmospheric vapor pressure (kPa) and $\dot{e}$ is $(e_i + e_a)/2$ (Gaastra, 1959; von Caemmerer & Farquhar, 1981; Cernusak *et al*., 2024). Sensitivity tests confirmed that, for the reported range of boundary layer conductance in *Pinus* species (2–2.84 mol m^{-2} s^{-1}; Cernusak *et al*., 2022), the g_s of trees in our study were low enough to largely control g_t variability; therefore, g_t was a suitable proxy for g_s. For measured δ^2H_{vapor}, δ^2H_{source}, $\delta^2H_{n\text{-}water}$ and $\Delta^2H_{n\text{-}water}$, we used data from Angove *et al*. (2023), where δ^2H_{source} was represented by twig water δ^2H. Since the time-integrated analyses required continuous δ^2H data throughout the growing season, we additionally modeled δ^2H_{source}, δ^2H_{vapor}, $\delta^2H_{n\text{-}water}$ and $\Delta^2H_{n\text{-}water}$ in PYTHON (van Rossum & Drake, 2009; Jupyter, 2022). This involved a mass-balanced-based model of water isotopes in the rooting zone for δ^2H_{source}, and leaf water heavy isotope enrichment modeling using the Craig–Gordon model and its different corrections (Péclet, two-pool and nonsteady state) for $\delta^2H_{n\text{-}water}$ and $\Delta^2H_{n\text{-}water}$ (Methods S2; Figs S2–S4). Model inputs included data from the ICOS carbon portal (Mammarella *et al*., 2024) and IsoGSM, an isotope-enabled atmospheric circulation model (Yoshimura *et al*., 2008, 2011). We also explored how accurately we could infer $\delta^2H_{n\text{-}water}$ from measured δ^2H_{alkane} in 1N and 0N. For this, we used the mean (−156‰), minimum (−133‰) and maximum (−192‰) isotope fractionation between $\delta^2H_{n\text{-}water}$ and δ^2H_{alkane} (ε_{bio}) reported by Hepp *et al*. (2021).

Data analyses

Data analysis was conducted in R (v.4.2.1; R Core Team, 2022). To explore how our δ^2H_{alkane} data aligns with previous studies, we inspected temporal trends in δ^2H values in all measured compounds and mixtures, and modeled $\delta^2H_{n\text{-}water}$ and δ^2H_{source}. We

© 2025 The Author(s).
New Phytologist © 2025 New Phytologist Foundation.

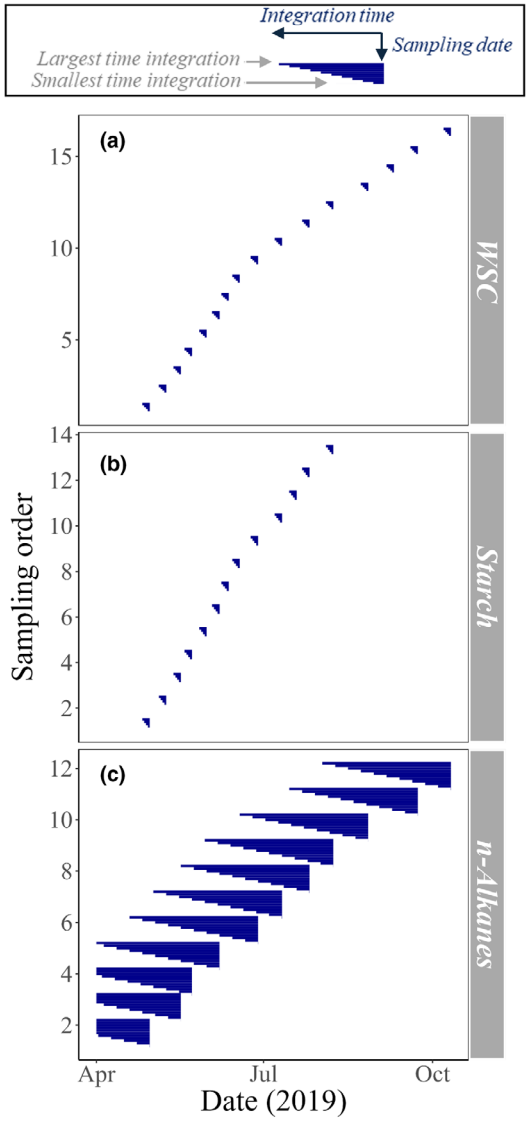

Fig. 1 Each sampling event, in chronological order (Sampling order), and the range of dates included in time-integrated analyses; for water-soluble carbohydrates (WSC) (a), starch (b) and *n*-alkanes (c), in *Pinus sylvestris* needles at Hyytiälä Forest.

then prepared time-integrated means of independent variables (Table 2). Data were filtered between 09:00 and 15:00 h, then averaged, and time integration was implemented during averaging. One day for time integration was represented by the mean of the sampling day, while a 2-d integration time was represented by an average of the sampling day and its preceding day. This was repeated for up to five integration days for δ^2H_{WSC} and δ^2H_{starch} (Fig. 1a,b), based on the WSC $\delta^{18}O$ integration time used for the same site (Leppä *et al.*, 2022), during the time window that coincided with our sampling period. For δ^2H_{alkane}, we used a period of 0–10 integration weeks to enhance the maximum time integration coverage and minimize exposure to uncertainties from the dormant winter period preceding the growing season (Fig. 1c). The starting date for modeled δ^2H_{source}, $\delta^2H_{n\text{-}water}$ and $\Delta^2H_{n\text{-}water}$ was 01 April 2019 because earlier starting dates were not in the scope of model validation since there is uncertainty in estimating winter tree water uptake for nonsteady state δ^2H_{source} predictions. Resultantly, the first three 1N sampling events had maximum time integrations of 4–5, 6–7 and 7–8 wk, respectively.

After integration times had been applied to selected independent variables (Table 2), they were compared with δ^2H_{WSC}, δ^2H_{starch} and δ^2H_{alkane} using Spearman's rank correlations. A Holm correction was applied to *P*-values for multiple integration day comparisons. The correlation results were visualized using an annotated color heat map, following the approach by Tang *et al.* (2024). We selected the independent factors, and their integration times, which were most strongly correlated with δ^2H_{WSC} and δ^2H_{alkane} for focused inspection by linear mixed models (LMMs). Since 1N δ^2H_{alkane} was related to multiple factors with negligible differences in rank relationship ($\rho < 0.04$), the focused LMM inspection featured the three factors most relevant to palaeohydrological reconstructions. Tree identity and sampling date were random intercept factors for δ^2H_{WSC} LMMs, but more parsimony was needed to validate an LMM for δ^2H_{alkane}; therefore, its random intercept was tree identity without sampling date. An 0N sampling event in October was not included in the LMM because the short integration period of δ^2H_{WSC} (Fig. 1a) was susceptible to bias from the October sampling event when the growing season had clearly ended.

Results

Concentrations of total lipid extracts and carbohydrates

Concentrations of WSCs, starch and TLE were typically higher in 1N than in 0N (Fig. 2a). There was a decline in WSC concentrations of 1N during the sampling period, from *c.* 160 to *c.* 80 mg g^{-1}. Meanwhile, in 0N, there was a small (*c.* 25 mg g^{-1}) decrease in WSC concentrations at the start of the sampling period, which then stabilized, and gradually increased between September and October, to *c.* 110 mg g^{-1}. Mean concentrations of TLE in 1N were relatively stable, varying between 139 and 156 mg g^{-1}. Meanwhile, in 0N, TLE concentration gradually increased from 100 to 150 mg g^{-1} to eventually reach equivalent concentrations to 1N, by the end of the sampling period. Starch concentrations in 1N peaked during mid-May. In 0N, starch concentrations were low (*c.* 3–20 mg g^{-1}) compared with all other measured concentrations, and they peaked in August (Fig. 2a).

The weight percentage of pinitol (a sugar alcohol) fraction in 1N WSC was rather invariable, ranging between 30% and 37% (Fig. 2b). Meanwhile, the 0N pinitol fraction declined from 51% to 36% during its sampling period, alongside decreases of 5% and 6% in glucose and fructose, respectively. These declines corresponded with an increase in the sucrose fraction from 30% to 51%.

Temporal trends in δ^2H

Needle gas exchange had a strong role in measured and modeled needle water δ^2H ($\delta^2H_{n\text{-}water}$), as both exhibited distinctly

© 2025 The Author(s).
New Phytologist © 2025 New Phytologist Foundation.

14698137, 0, Downloaded from https://nph.onlinelibrary.wiley.com/doi/10.1111/nph.20448 by Luonnonvarakeskus, Wiley Online Library on [24/02/2025]. See the Terms and Conditions (https://onlinelibrary.wiley.com/terms-and-conditions) on Wiley Online Library for rules of use; OA articles are governed by the applicable Creative Commons License

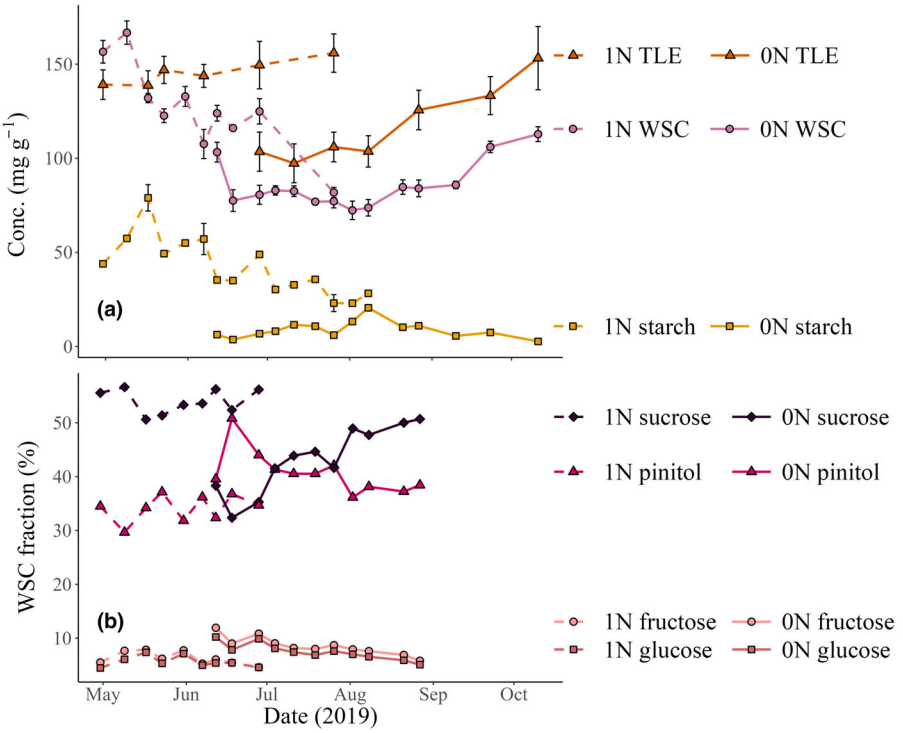

Fig. 2 Time series of concentration and composition changes in carbohydrates and total lipid extracts (TLE). (a) Concentration of TLE, water-soluble carbohydrates (WSC) and starch, in 1-yr-old needles (1N) and current-year needles (0N), during their respective sampling periods. Error bars represent SE, which was not always available for starch because its low concentrations required sample pooling. (b) Percentage contribution of different WSC constituents to the bulk WSC pool in 1N and 0N. Data from five *Pinus sylvestris* trees at Hyytiälä Forest, central Finland.

different and larger variability compared to measured and modeled twig water δ^2H (δ^2H_{source}; Fig. 3a). In late September, δ^2H_{source} was underestimated, as reported for $\delta^{18}O_{source}$ (Leppä *et al.*, 2022). Nonetheless, it did not bias modeled $\delta^2H_{n\text{-}water}$ (Fig. 3a). When measured δ^2H_{source} and δ^2H_{vapor} were missing, the predictions for $\delta^2H_{n\text{-}water}$ were moderately accurate (Fig. S5; Table S1). This was substantial accuracy for this study to implement multiday or multiweek time-integrated comparisons to organic δ^2H variability (Fig. 3). When exploring $\delta^2H_{n\text{-}water}$ predictions from δ^2H_{alkane} using mean (−156‰) to minimum (−133‰) reported ε_{bio} values, $\delta^2H_{n\text{-}water}$ from 1N δ^2H_{alkane} was, at a low resolution, within the general range and direction of measured 1N $\delta^2H_{n\text{-}water}$ (Fig. 3a). But $\delta^2H_{n\text{-}water}$ from 0N δ^2H_{alkane} did not capture the general variability observed in measured 1N $\delta^2H_{n\text{-}water}$. $\delta^2H_{n\text{-}water}$ predictions from the maximum reported ε_{bio} value (−192‰), not shown, were highly unrealistic; at *c.* −6 to 6 from 1N δ^2H_{alkane} and 4–15‰ from 0N δ^2H_{alkane}.

When 1N δ^2H_{WSC} overlapped with 0N δ^2H_{WSC} measurements, δ^2H_{WSC} was lower in 1N than in 0N (Fig. 3b). In 1N, δ^2H_{WSC} was significantly (18‰; $P < 0.01$; $t = -3.94$; $n = 10$) lower than δ^2H_{starch}, on sampling days when they were both analyzed. However, this was not reciprocated in the few pairwise measurements available for 0N ($P > 0.05$; $t = 1.86$; $n = 4$). δ^2H_{starch} in 0N, the most variable of all organic compound pools (Table 3), began with high values ($\delta^2H \approx -132$‰) close to the mean branch phloem δ^2H_{WSC} (−137.5‰) at the start of 0N sampling, followed by a steep decrease to *c.* −238‰, interspersed by a relatively small increase during July. In 1N, the δ^2H_{starch} and δ^2H_{WSC} both generally decreased during the growing season, sharing some peaks and troughs at similar sampling points, albeit more subtly for δ^2H_{WSC}. Similarly, δ^2H_{alkane} gradually decreased in 1N, from −185‰ to −199‰.

Unlike for δ^2H_{WSC} and δ^2H_{starch}, the interquartile range for δ^2H_{alkane} had a negligible difference between needle ages (0.5‰), and its interquartile range was as low as the less variable range of δ^2H_{source} (11‰). On average, δ^2H_{alkane} was the most depleted of all measured organic compounds and mixtures (Fig. 3b; Table 3). Notably, it was not lower than δ^2H_{WSC} in 0N at the end of the growing season (Fig. 3b).

Mean isotope fractionation between modeled $\delta^2H_{n\text{-}water}$ and leaf organic compound δ^2H (following eqn 4 in Holloway-Phillips *et al.*, 2022) is given in Table S2, but these are approximate estimates because of the variable integration times of different organic compounds.

Nonstructural carbohydrate δ^2H relationships to time-integrated factors

The Spearman's correlations between δ^2H and selected factors (Table 2) varied between needle generation, and between WSC and starch (Fig. 4). In both 1-yr-old needles (1N) and current-year needles (0N), δ^2H_{WSC} was most strongly correlated with A_n ($P < 0.05$). However, the trends were opposite: 0N was positively related to A_n ($\rho = 0.89$), while 1N was negatively correlated with A_n ($\rho = -0.82$). The optimal integration time for both needle ages was 2–3 d, and both days had strong correlations for both needle ages. In addition to the strong correlations between δ^2H_{WSC} and time-integrated A_n, δ^2H_{WSC} was, to a lesser extent, significantly related to modeled 1N $\delta^2H_{n\text{-}water}$ and $\Delta^2H_{n\text{-}water}$ in both needle ages. Just as 1N δ^2H_{WSC} was negatively related to time-integrated A_n while 0N δ^2H_{WSC} was positively related to

© 2025 The Author(s).
New Phytologist © 2025 New Phytologist Foundation.

14698137, 0, Downloaded from https://nph.onlinelibrary.wiley.com/doi/10.1111/nph.20448 by Luonnonvarakeskus, Wiley Online Library on [24/02/2025]. See the Terms and Conditions (https://onlinelibrary.wiley.com/terms-and-conditions) on Wiley Online Library for rules of use; OA articles are governed by the applicable Creative Commons License

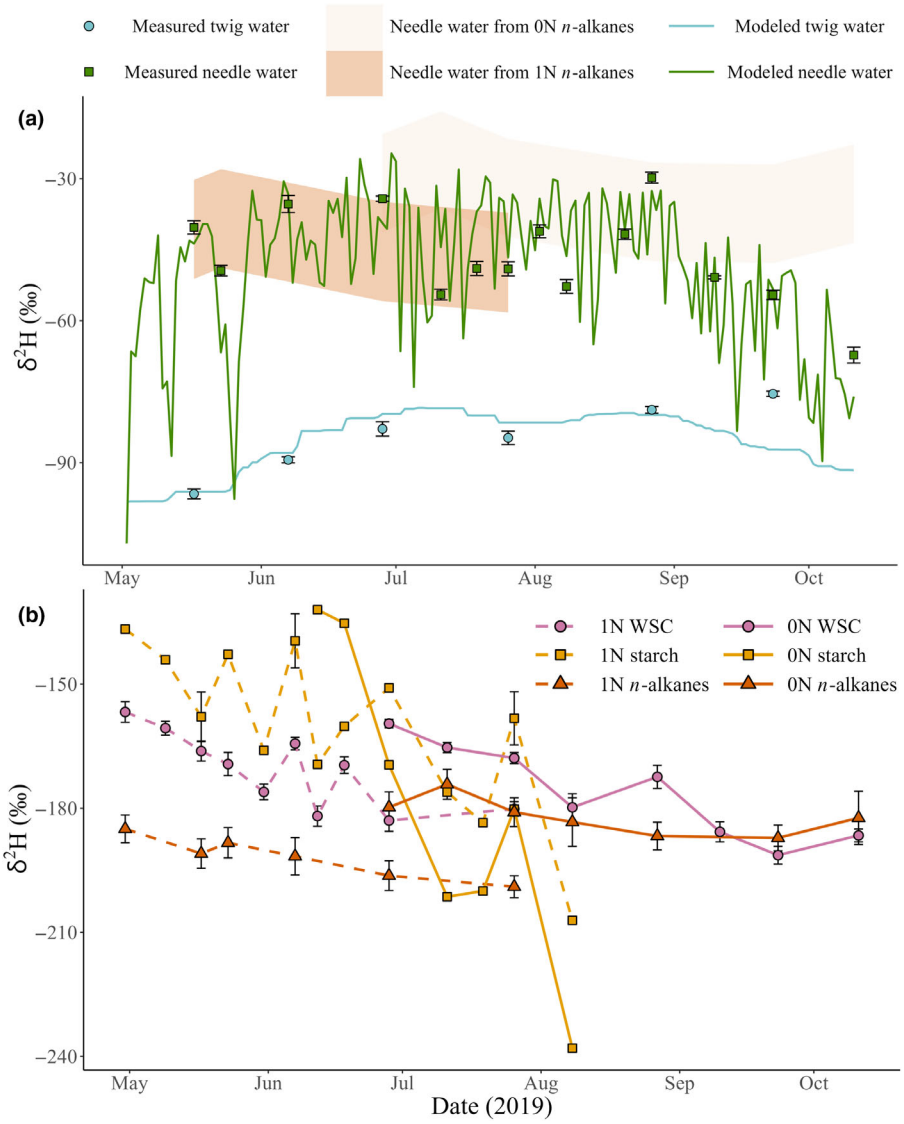

Fig. 3 Temporal variability of δ^2H in different compounds and mixtures from 1-yr-old (1N) and current-year (0N) needles of five *Pinus sylvestris* trees during the 2019 growing season at Hyytiälä forest, central Finland. (a) Measured δ^2H of 1-yr-old needle water (green datapoints; 1N $\delta^2H_{n\text{-water}}$) with its modeled values (green line; Craig–Gordon model with Péclet correction), and measured twig water δ^2H (blue datapoints; δ^2H_{source}), with the modeled values used for gap filling (blue line; mass balanced-based model of the rooting zone). Shaded areas (orange) show $\delta^2H_{n\text{-water}}$ when inferred from *n*-alkane δ^2H (δ^2H_{alkane}) using the mean (−156‰) and minimum (−133‰) isotope fractionation between $\delta^2H_{n\text{-water}}$ and δ^2H_{alkane} (ε_{bio}) reported by Hepp *et al*. (2021). (b) δ^2H of water-soluble carbohydrates (WSC, δ^2H_{WSC}), starch (δ^2H_{starch}) and *n*-alkanes in 1-yr-old needles (1N; dashed lines) and current-year needles (0N; solid lines). Error bars show SE, which was not always available for δ^2H_{starch} because of sample pooling, to accommodate low starch concentrations.

Table 3 Means (±SE) and interquartile ranges of δ^2H (‰) in different compounds and mixtures.

	Twig	Current-year needles	One-year-old needles	Branch phloem
Mean ± SE				
Water	−84.8 ± 1.3	–	−45.1 ± 1.4	–
WSC	–	−176.1 ± 1.9	−170.6 ± 1.4	−137.5 ± 2.3
Starch	–	−179.5 ± 14.3	−155.6 ± 3.6	−73.7 ± 2.7
n-Alkanes	–	−182.4 ± 1.6	−192.5 ± 1.5	–
Interquartile range				
Water	11	–	15.7	–
WSC	–	21.2	14.6	12.7
Starch	–	48.3	24.3	4.4
n-Alkanes	–	11	11.5	–

Data from five *Pinus sylvestris* trees monitored during 2019, at Hyytiälä Forest, central Finland. WSCs, water-soluble carbohydrates.

time-integrated A_n, 1N δ^2H_{WSC} had a negative relationship with modeled 1N $\delta^2H_{n\text{-water}}$ while 0N δ^2H_{WSC} had a positive relationship. δ^2H_{WSC} was most strongly related to modeled 1N $\delta^2H_{n\text{-water}}$ after four integration days for 1N ($\rho = -0.31$), and 2 d for 0N ($\rho = 0.82$). Meanwhile, δ^2H_{WSC} was positively correlated with modeled 1N $\Delta^2H_{n\text{-water}}$ in both needle ages, and the strongest correlations were after 4 d for 1N ($\rho = 0.78$), and 2 d for 0N ($\rho = 0.86$). Exclusively for 0N, the strongest signals in

© 2025 The Author(s).
New Phytologist © 2025 New Phytologist Foundation.

14698137, 0, Downloaded from https://nph.onlinelibrary.wiley.com/doi/10.1111/nph.20448 by Luonnonvarakeskus, Wiley Online Library on [24/02/2025]. See the Terms and Conditions (https://onlinelibrary.wiley.com/terms-and-conditions) on Wiley Online Library for rules of use; OA articles are governed by the applicable Creative Commons License

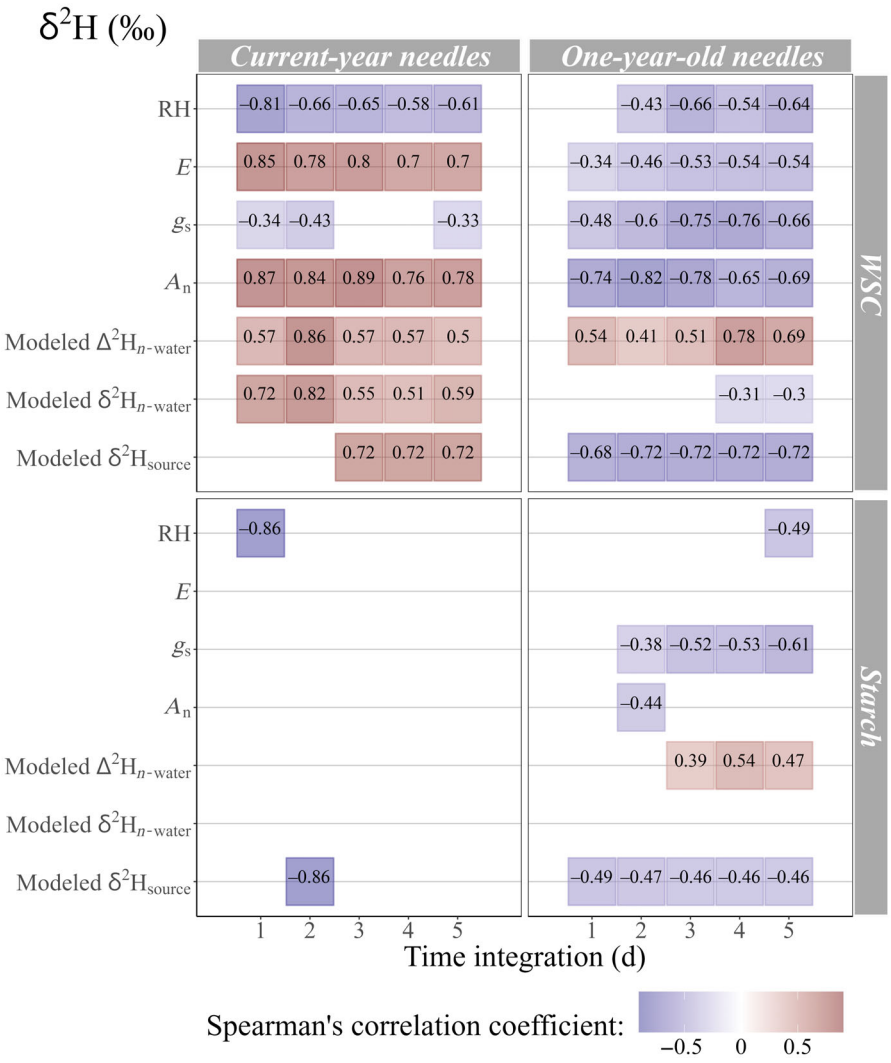

Fig. 4 Time-integrated Spearman's correlations identifying physiological and environmental signals in nonstructural carbohydrate δ^2H (water-soluble carbohydrate δ^2H (WSC) and starch δ^2H). Up to 5 d of time integration are used, based on evidence from WSC $\delta^{18}O$ for the specific spatiotemporal context of this study (Leppä *et al*., 2022). Physiological factors include the following: transpiration rate (E, mol m^{-2} s^{-1}), stomatal conductance (g_s, mol m^{-2} s^{-1}) and net assimilation rate (A_n, μmol m^{-2} s^{-1}). Environmental factors include the following: relative humidity (RH, %), modeled needle water ^2H enrichment ($\Delta^2H_{n\text{-water}}$, ‰), modeled needle water δ^2H ($\delta^2H_{n\text{-water}}$, ‰) and modeled source water δ^2H (δ^2H_{source}, ‰). Isotope measurements are from current-year needles (0N) and 1-yr-old needles (1N) of five *Pinus sylvestris* trees monitored throughout the 2019 growth season, while gas exchange data are from continuous mature needle cuvette measurements at half-hourly resolution, at Hyytiälä Forest, central Finland.

δ^2H_{WSC} were closely followed by RH and E, which were strongest on the day of sampling (Fig. 4).

δ^2H_{starch} in 0N was most strongly correlated with δ^2H_{source} after a 2-d integration ($\rho = -0.86$) and RH on the sampling day ($\rho = -0.86$; Fig. 4). By contrast, in 1N, the strongest relationship was a weak correlation with g_s after five integration days ($\rho = -0.61$, $P < 0.05$).

Linear mixed models confirmed a strong positive relationship between time-integrated A_n (T:A_n) and 0N δ^2H_{WSC} within the growing season (Table 4; Fig. 5a). By contrast, for 1N, the relationship was weaker and negative. Although δ^2H_{WSC} decreased in both 0N and 1N throughout the growing season, A_n increased in 1N while δ^2H_{WSC} decreased (Fig. 5b). Meanwhile, in 0N, the decrease in A_n closely aligned with the decrease in δ^2H_{WSC} toward the end of the growing season (Fig. 5b).

n-Alkane δ^2H relationships to time-integrated factors

0N δ^2H_{alkane} was not significantly correlated with modeled $\delta^2H_{n\text{-water}}$ at any time integration ($P > 0.05$; Fig. 6). Instead, it had a weak negative relationship to modeled δ^2H_{source} that became stronger as the time integration increased to 10 wk ($\rho = -0.39$, $P < 0.05$). It was also weakly correlated with A_n, after 5 and 6 integration weeks ($\rho = 0.35$, $P < 0.05$). The weak relationship between 0N δ^2H_{alkane} and δ^2H_{source} after 10 wk of integration (Figs 6, 7b) did not fulfill the model validation requirements for a generalized LLM. There were noticeable inter-tree differences in δ^2H_{alkane}, for both needle ages, indicated by the relatively large vertical scatter in Fig. 7.

1N δ^2H_{alkane} exhibited stronger correlations to tested factors compared to 0N δ^2H_{alkane} (Fig. 6). It was correlated with a subselection of the factors tested (Table 2). The prevailing signals in 1N δ^2H_{alkane} were RH, δ^2H_{source}, $\delta^2H_{n\text{-water}}$, A_n and g_s, and their rank (ρ) differences were < 0.04 (Fig. 6). In most cases, the strongest signals were observed between 5 and 10 integration weeks, except that δ^2H_{source} exhibited an invariable ($\rho < 0.02$) signal between 2 and 10 wk. The LLM that compared 1N δ^2H_{alkane} with hydrological factors (T:$\delta^2H_{n\text{-water}}$, T:δ^2H_{source}, RH) identified a high likelihood (46–47%) that δ^2H_{alkane} from the same tree would correlate (Table 4). Excluding the role of tree identity in the relationship between 1N δ^2H_{alkane} and T:$\delta^2H_{n\text{-water}}$ (random intercept model), there was a weak (R^2(M)

© 2025 The Author(s).
New Phytologist © 2025 New Phytologist Foundation.

14698137, 0, Downloaded from https://nph.onlinelibrary.wiley.com/doi/10.1111/nph.20448 by Luonnonvarakeskus, Wiley Online Library on [24/02/2025]. See the Terms and Conditions (https://onlinelibrary.wiley.com/terms-and-conditions) on Wiley Online Library for rules of use; OA articles are governed by the applicable Creative Commons License

New Phytologist

Table 4 Linear mixed model fits for time-integrated signals (net assimilation rate, $T{:}A_n$, μmol m^{-2} s^{-1}; modeled needle water δ^2H, $T{:}\delta^2H_{n\text{-}water}$, ‰; gap filled source water δ^2H, $T{:}\delta^2H_{source}$, ‰) in water-soluble carbohydrate δ^2H (δ^2H_{WSC}) and *n*-alkane δ^2H (δ^2H_{alkane}), in current-year needles (0N) and 1-yr-old needles (1N) from five *Pinus sylvestris* trees at Hyytiälä Forest, central Finland.

Regressor	Response	Intercept	Slope	ICC	R^2(M)	R^2(C)
3-d $T{:}A_n$	0N δ^2H_{WSC}	−246.78 ± 6.56	**17.11** ± 1.49	0.13	0.8	0.93
2-d $T{:}A_n$	1N δ^2H_{WSC}	−123.52 ± 7.29	**−10.88** ± 1.64	0.18	0.66	0.84
10-wk T:RH	1N δ^2H_{alkane}	−134.38 ± 9.17	**−1.13** ± 0.17	0.47	0.31	0.77
5-wk $T{:}\delta^2H_{n\text{-}water}$		−234.93 ± 7.42	**−0.85** ± 0.14	0.47	0.29	0.75
5-wk $T{:}\delta^2H_{source}$		−246.02 ± 9.12	**−0.59** ± 0.1	0.46	0.29	0.75

Bold when significant ($P < 0.05$). ICC, intraclass correlation; R^2(C), conditional R^2; R^2(M), marginal R^2; RH, relative humidity; WSC, water-soluble carbohydrates.

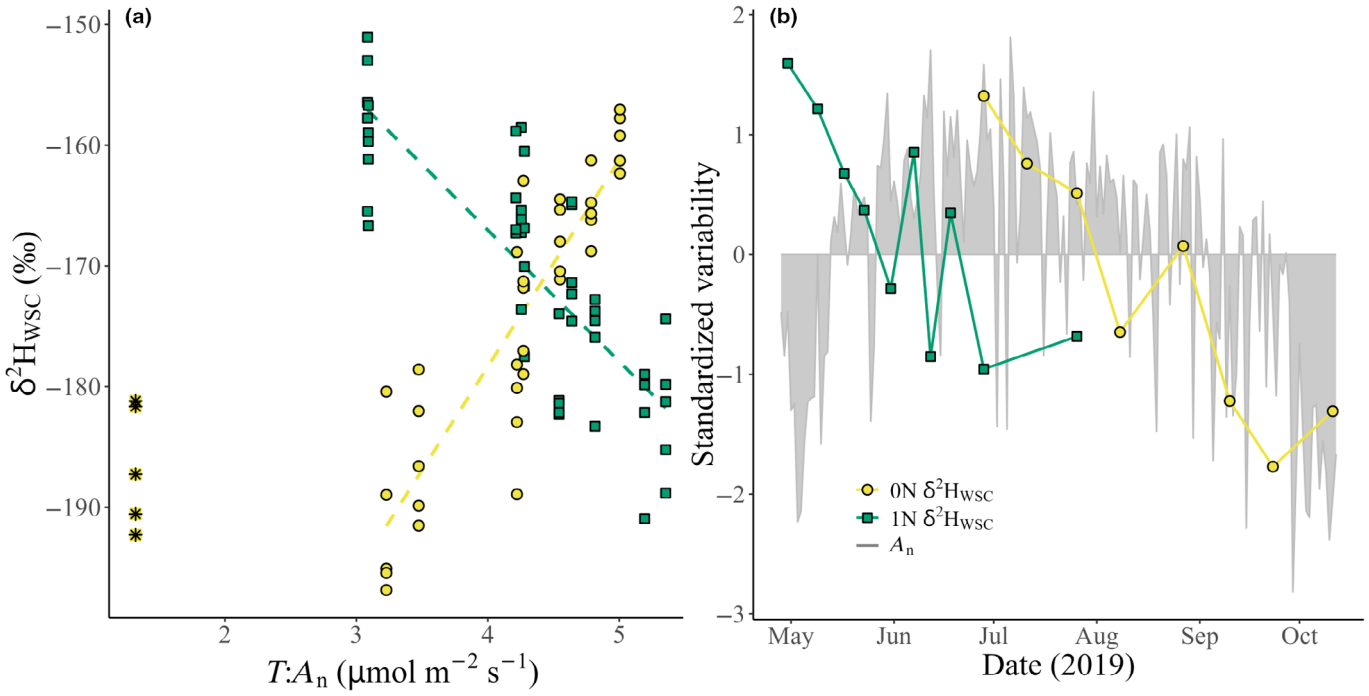

Fig. 5 Water-soluble carbohydrate (WSC) δ^2H (δ^2H_{WSC}) relationships to net assimilation rate (A_n, μmol m^{-2} s^{-1}), for current-year needles (0N, yellow series) and 1-yr-old needles (1N, green series) from five *Pinus sylvestris* trees at Hyytiälä Forest, central Finland. A_n data are from continuous 1N needle cuvette measurements at half-hourly resolution. In (a), A_n is time integrated ($T{:}A_n$) to 3 d for 0N (R^2(M) = 0.8, $P < 0.05$) and 2 d for 1N (R^2(M) = 0.66, $P < 0.05$), dashed lines show significant linear mixed model fits, and asterisks show an 0N δ^2H_{WSC} outlier from a sampling day in October, when the growing season had ended. In (b), A_n is not time-integrated, and each of the variables were standardized (centered (mean of a variable subtracted from its values) and then scaled (divided by the SD, for each variable)).

= 0.29) negative relationship; a trend that was mirrored by the relationship between 1N δ^2H_{alkane} and $T{:}\delta^2H_{source}$ albeit with a milder gradient (Fig. 7d,e; Table 4). The relationship was marginally stronger (R^2(M) = 0.31) for RH (Fig. 7f; Table 4).

Discussion

Our study is the first to investigate time-integrated, physiological and environmental signals in δ^2H of *n*-alkanes and carbohydrates in a natural forest during a growing season. This was feasible from an intensive field survey of a highly monitored site (ICOS, SMEAR), supported by modeling for gap-filling missing measured data. Nonetheless, our results cannot provide the causality achieved from a controlled glasshouse experiment. Instead, they contextualize the role of different factors influencing δ^2H amidst multiple seasonally variable factors occurring at natural frequencies. We show that, in a natural boreal forest, prevailing intraseasonal physiological and environmental signals can be identified from δ^2H_{alkane}, δ^2H_{WSC} and δ^2H_{starch} after accounting for an integration time of days or weeks.

n-Alkane δ^2H relationships to hydrological factors were regulated by physiological processes

0N δ^2H_{alkane} did not have a substantial relationship with δ^2H of any of the water pools investigated (Figs 6, 7). The strongest

© 2025 The Author(s).
New Phytologist © 2025 New Phytologist Foundation.

14698137, 0, Downloaded from https://nph.onlinelibrary.wiley.com/doi/10.1111/nph.20448 by Luonnonvarakeskus, Wiley Online Library on [24/02/2025]. See the Terms and Conditions (https://onlinelibrary.wiley.com/terms-and-conditions) on Wiley Online Library for rules of use; OA articles are governed by the applicable Creative Commons License

14698137, 0, Downloaded from https://nph.onlinelibrary.wiley.com/doi/10.1111/nph.20448 by Luonnonvarakeskus, Wiley Online Library on [24/02/2025]. See the Terms and Conditions (https://onlinelibrary.wiley.com/terms-and-conditions) on Wiley Online Library for rules of use; OA articles are governed by the applicable Creative Commons License

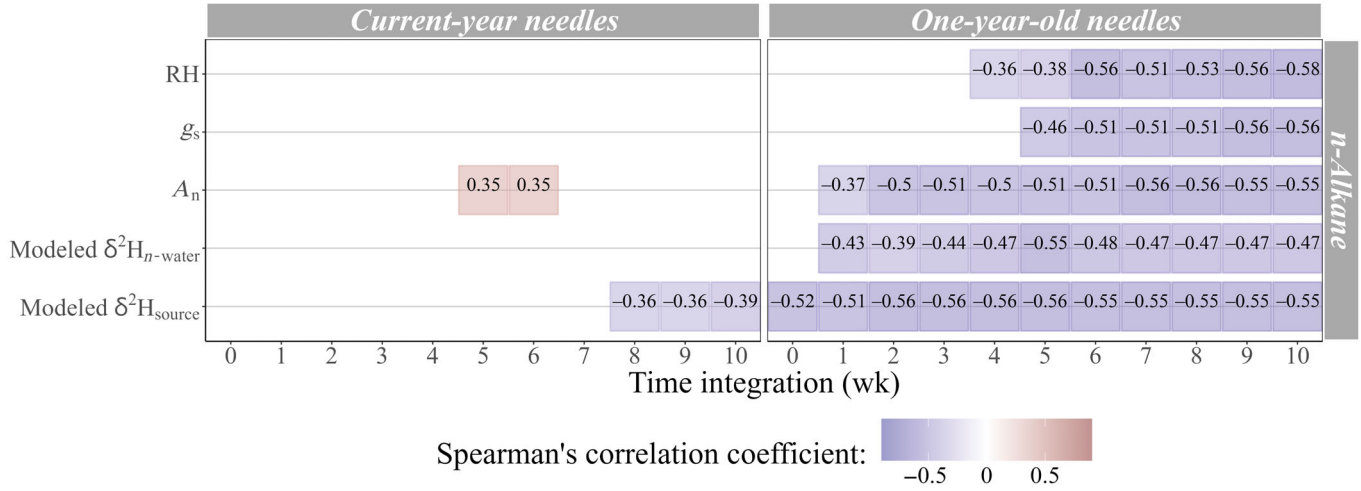

Fig. 6 Significant time-integrated Spearman's correlations between *n*-alkane δ^2H and the following factors: relative humidity (RH) (%), stomatal conductance (g_s, mol m^{-2} s^{-1}), net assimilation rate (A_n, μmol m^{-2} s^{-1}), modeled needle water δ^2H ($\delta^2H_{n\text{-water}}$, ‰) and modeled source water δ^2H (δ^2H_{source}, ‰). *n*-Alkane δ^2H is from current-year needles (0N) and 1-yr-old needles (1N) of five *Pinus sylvestris* trees monitored during 2019 at Hyytiälä Forest, central Finland. Gas exchange data are from continuous mature needle cuvette measurements at half-hourly resolution.

observed relationship was a weak Spearman's rank correlation ($\rho = -0.39$) to δ^2H_{source} after 8–10 wk of time integration. This supports previous evidence that δ^2H_{alkane} is strongly affected by complex biosynthetic ^{2}H-fractionation (Baan *et al.*, 2023a). Furthermore, one of the two remaining factors related to 0N δ^2H_{alkane}, after T:δ^2H_{source}, was T:A_n (3 or 5 wk), which had a weak positive correlation ($\rho = 0.35$; Fig. 6). Its weak positive trend could have indicated a switch from heterotrophy to autotrophy (Tipple & Ehleringer, 2018), and the absence of a $\delta^2H_{n\text{-water}}$ signal might have been due to incomplete autotrophy (Zhu *et al.*, 2020). Another potential reason is that gas-exchange data were not available for 0N, and inaccuracies could have been introduced by using gas-exchange data from older needle generations, but the multiweek averaging that covered large seasonal change, likely superseded gas-exchange differences between needle ages (Fig. S1). The different origins of NADPH used for *n*-alkane synthesis (Cormier *et al.*, 2018; Wijker *et al.*, 2019; Maloney *et al.*, 2024), relating to biochemical fluxes, could have also contributed to the large intertree differences in δ^2H_{alkane} in both 0N and 1N.

1N δ^2H_{alkane} was related to a subselection of factors (RH, δ^2H_{source}, A_n, g_s and $\delta^2H_{n\text{-water}}$), which had marginal differences in signal strength (Fig. 6). Relative humidity was marginally the strongest signal (Figs 6, 7), which could have stemmed from its indirect relationships to both $\delta^2H_{n\text{-water}}$ and δ^2H_{source} (Cernusak *et al.*, 2022; Methods S2). Interestingly, 1N δ^2H_{alkane} were negatively related to $\delta^2H_{n\text{-water}}$ (Figs 6, 7), which suggests variability in biosynthetic isotope fractionation playing a significant role during the imprinting of hydrological signals to δ^2H_{alkane} (Baan *et al.*, 2023a). A potential explanation is that higher $\delta^2H_{n\text{-water}}$ indicated favorable evaporative conditions, which promoted the use of more chloroplast-derived NADPH for wax synthesis, which is likely more ^{2}H-depleted than in cytosol-derived NADPH (Sessions *et al.*, 1999); more details on potential changes in lipid biosynthesis pathways can be found in Zhou *et al.* (2016). Furthermore, δ^2H_{alkane} includes a δ^2H signal from both chloroplastic water and cytosolic water – any variability in the contributions from these water pools could influence δ^2H_{alkane} (Holloway-Phillips *et al.*, 2022). Since chloroplastic and cytosolic waters are assumed to comprise different proportions of water exposed to evaporative enrichment (Barbour & Farquhar, 2000; Cernusak *et al.*, 2004; Holloway-Phillips *et al.*, 2022), changes in their relative contributions to δ^2H_{alkane} would lead to fluctuations in δ^2H_{alkane} between enriched and unenriched leaf water, perhaps partly reflected here as fluctuations between $\Delta^2H_{n\text{-water}}$ and $\delta^2H_{n\text{-water}}$. Nonetheless, since δ^2H_{alkane} was negatively related to both $\delta^2H_{n\text{-water}}$ and δ^2H_{source} (Figs 6, 7; Table 4), water compartmentation and heterogeneity are not likely as temporally influential to δ^2H_{alkane} compared with other sources of variability, including sourcing NADPH and other precursor molecules from long-term storage. Accordingly, it was interesting to observe A_n and g_s signals in 1N δ^2H_{alkane}, after time integration periods beyond 1 and 5 wk, respectively (Fig. 6).

Ultimately, it was not expected to find a relationship with $\delta^2H_{n\text{-water}}$ in 1N, because δ^2H_{alkane} was supposedly from only the early stages of needle growth. However, Ofiti *et al.* (2023) showed that needles from different years of the conifer *Picea mariana* had the same *n*-alkane concentration responses to a warming treatment. This suggests that *de novo* biosynthesis of *n*-alkanes in mature needles might be substantial enough for needle δ^2H_{alkane} to respond to environmental variability and be a more reliable indicator of processes correlating with $\delta^2H_{n\text{-water}}$. This could be a result of less 1N exposure to variability in biosynthetic fractionation (Sachse *et al.*, 2015; Tipple & Ehleringer, 2018), such as variability in the synthesis pathway for NADPH-derived H atoms (Zhou *et al.*, 2016; Maloney *et al.*, 2024). This could have been interlinked with a lower dependency on precursor

© 2025 The Author(s).
New Phytologist © 2025 New Phytologist Foundation.

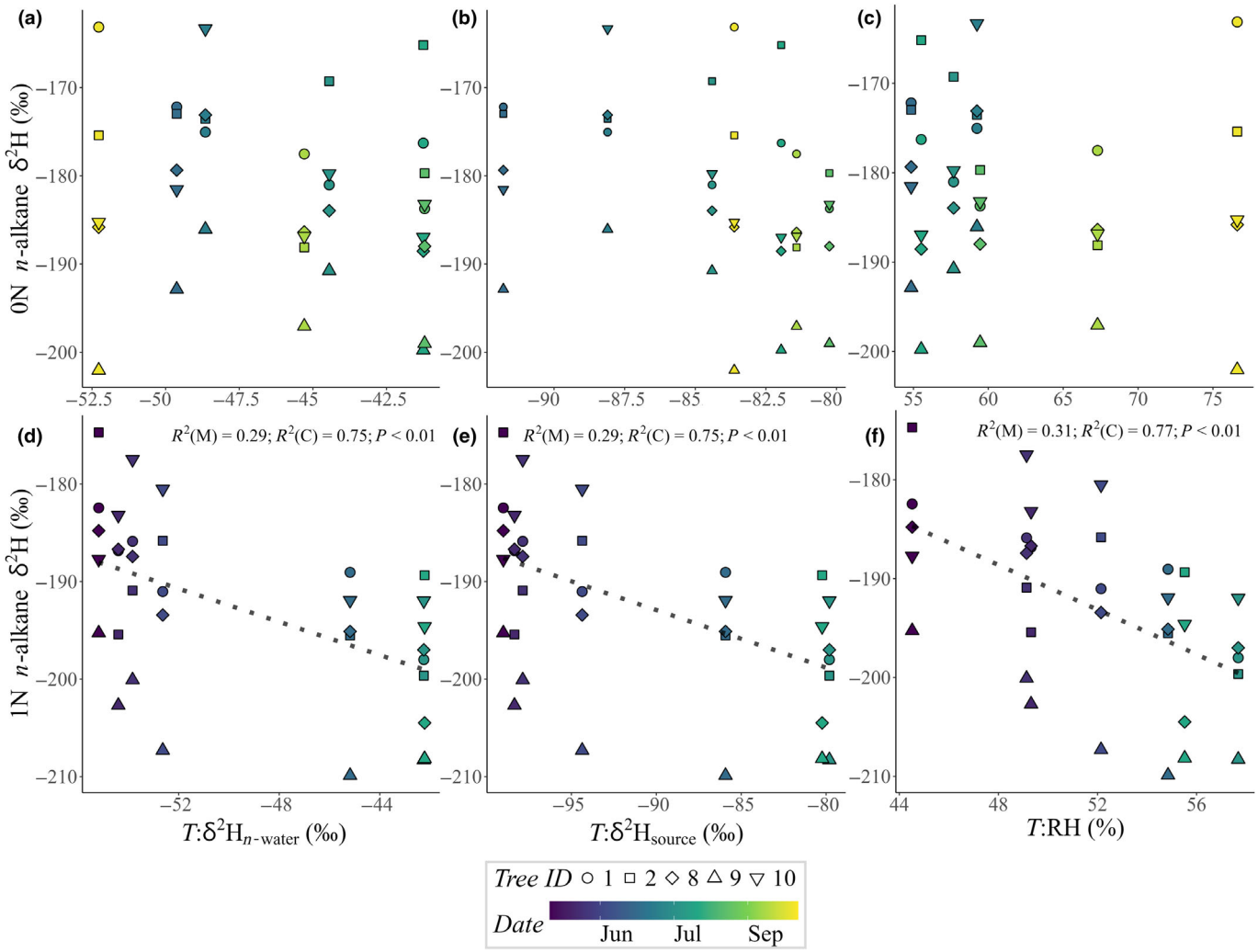

Fig. 7 Needle *n*-alkane δ^2H (‰) relationships to time-integrated δ^2H in water pools and relative humidity (RH), to examine hydrological signals in *n*-alkane δ^2H when at their strongest. Current-year needle (0N) *n*-alkane δ^2H relationships to 10-wk integrated (a) modeled needle water δ^2H (T:$\delta^2H_{n\text{-water}}$, ‰), (b) gapfilled source water δ^2H (T:δ^2H_{source}, ‰) and (c) atmospheric relative humidity (T:RH, %). One-year-old needle (1N) *n*-alkane δ^2H relationships to 5-wk integrated (d) T:$\delta^2H_{n\text{-water}}$ (‰), (e) T:δ^2H_{source} (‰) and (f) 10-wk integrated T:RH (%), with dashed lines showing significant linear mixed model fits. Data are from five *Pinus sylvestris* trees at Hyytiälä Forest, central Finland, during 2019.

molecules originating from long-term storage, which additionally have different isotopic signals (Lehmann *et al.*, 2024b). Since mature needles are generally those that senesce, this is a promising message for the interpretation of δ^2H_{alkane}, because this might represent processes related to a time-integrated evaporative signal from the duration of the needle lifespan. Our data are in line with other studies observing a renewal of needle alkanes during their lifespan (Ofiti *et al.*, 2023), similar to other plant types (Srivastava & Wiesenberg, 2018; Speckert *et al.*, 2023). As the alkane concentrations do not increase during the lifetime of leaves, this argues for a release of these epicuticular compounds into the environment as aerosols (Conte & Weber, 2002). Likely, the majority of these alkanes enter the soil in the vicinity of their plants, thus contributing an alkane signal from presenescent leaves, capturing the time until they are released. However, there is scarce information on the renewal rates of alkanes in needles (Ofiti *et al.*, 2023) and leaves (Speckert *et al.*, 2023) of mature trees, which hampers a quantitative assessment of the contribution of senesced needles compared with living needles to the soil alkane pool. Until such information is available, we have to keep in mind that the soil alkane composition is a composite of the alkane signal that we measure on tree biomass, despite the promising results we received in the current study.

Water-soluble carbohydrate δ^2H can have mixed relationships to A_n

This is the first study to relate needle gas exchange to δ^2H_{WSC} in a natural forest. The relationships between T:A_n and δ^2H_{WSC} support findings from glasshouse experiments showing that leaf gas exchange, such as dark respiration and net photosynthesis, has a strong role in sugar δ^2H (Holloway-Phillips *et al.*, 2022).

© 2025 The Author(s).
New Phytologist © 2025 New Phytologist Foundation.

14698137, 0, Downloaded from https://nph.onlinelibrary.wiley.com/doi/10.1111/nph.20448 by Luonnonvarakeskus, Wiley Online Library on [24/02/2025]. See the Terms and Conditions (https://onlinelibrary.wiley.com/terms-and-conditions) on Wiley Online Library for rules of use; OA articles are governed by the applicable Creative Commons License

14698137, 0, Downloaded from https://nph.onlinelibrary.wiley.com/doi/10.1111/nph.20448 by Luonnonvarakeskus, Wiley Online Library on [24/02/2025]. See the Terms and Conditions (https://onlinelibrary.wiley.com/terms-and-conditions) on Wiley Online Library for rules of use; OA articles are governed by the applicable Creative Commons License

We show that physiology, in this case A_n, can be the predominant signal in needle δ^2H_{WSC} in a natural boreal forest (Figs 4, 5). Gas-exchange measurements were not available for 0N, and correlations for 0N were performed using needle gas exchange data from mature needles, which may have affected the outcomes. Nonetheless, the seasonal variability in A_n was likely much larger than needle generation differences (Figs 5b, S1), and there were relatively strong E and RH signals observed in 0N δ^2H_{WSC} (Fig. 4). Overall, given that the 1N and 0N sampling periods cover different parts of the growing season, there are multiple potential mechanistic reasons for their differences. For example, the positive relationship between δ^2H_{WSC} in 0N and A_n could be because they coincided with an increasing sugar pool size (Fig. 2a), and if it subsequently had a lower turnover rate, then the sugar pool could have been more exposed to ^2H enrichment by H atom exchange with surrounding needle water (Holloway-Phillips *et al.*, 2022). The WSC pool is likely exposed for extended periods of time in a natural forest because our study, and Leppä *et al.* (2022) suggest that the WSC pool can be an accumulation from multiple days. To evaluate the role of turnover rate to δ^2H_{WSC} in a natural forest, implementation of non-steady state WSC isotope modeling is needed to determine the age of the 0N WSC pool, and its interactions with δ^2H_{WSC}. Another potential explanation for the relationship between T:A_n and 0N δ^2H_{WSC} is the seasonal increase in the sucrose fraction of the WSC pool (Fig. 2b); if it was more ^2H depleted, it could have contributed to the decreasing δ^2H_{WSC} trend (Abrahim *et al.*, 2020). Notably, the relative levels of sucrose and other constituents remained constant in 1N (Fig. 2b).

The inverse relationship between A_n and δ^2H_{WSC} in 1N can be more pragmatically explained than in 0N; wherein the higher ratio between photosynthetic rate and respiration led to an accumulation of ^2H-depleted sugars not consumed by respiration. That is, there may have been less impact from potential ^2H-enrichment of triose phosphates by glyceraldehyde 3-phosphate (GADPH) in the cytosol, by a reduced relative flux of triose phosphates for respiration (Wieloch *et al.*, 2024). This supports the hypothesis that the partitioning of triose phosphates has an associated isotope fractionation influential enough to affect triose phosphate δ^2H, which in turn affects sugar δ^2H (Holloway-Phillips *et al.*, 2022). Nonetheless, while GADPH imprints a $\delta^{13}C$ signal to glucose (Wieloch *et al.*, 2021), its role in δ^2H in sugars still needs to be examined, alongside other potential pathways. Alternatively, if the increase in A_n was related to a decrease in dark respiration, a decrease in futile sucrose cycling could have reduced H-exchange with water (Geigenberger & Stitt, 1991; Holloway-Phillips *et al.*, 2022; Lehmann *et al.*, 2024b).

Overall, if both needle ages contribute to the phloem pool for cellulose development during their respective measurement periods, the mixed relationships between needle δ^2H_{WSC} and A_n complicate the interpretation of tree-ring δ^2H, which is known to record tree stress responses (Lehmann *et al.*, 2021; Vitali *et al.*, 2022, 2023). Therefore, future studies need to trace needle sugar δ^2H to the phloem to discern the fate of different δ^2H_{WSC} signals that can vary with needle age and seasonality (Gessler *et al.*, 2013).

Starch δ^2H has unique relationships to physiological and environmental factors

Starch concentrations and their $\delta^{13}C$ values show that the dynamic needle starch pool is rapidly used for metabolic processes and is sensitive to resource availability (Yan *et al.*, 2012; Desalme *et al.*, 2017). These findings are reciprocated by root starch $\delta^{13}C$ values from the same forest as this study (Tang *et al.*, 2022). Based on the dynamic starch concentrations (Fig. 2a) and δ^2H_{starch} (Fig. 3b) observed here, most of the starch likely originates from newly assimilated carbon. In 0N, most starch was likely transitory because time-integrated analyses (Fig. 4) revealed that the strongest environmental signals in δ^2H_{starch} were observed after only 1 (RH, $\rho = -0.86$) or 2 (δ^2H_{source}, $\rho = -0.86$) days. Whereas in 1N, starch was likely less dominated by transitory starch, and included a representative portion of long-term starch storage, as indicated by weaker signals, which were highest after longer integration times than in 0N (e.g. g_s; highest after 5 integration days; $\rho = -0.61$). These findings are supported by the relatively higher starch concentrations in 1N than in 0N (Fig. 2a). It has been hypothesized that the seasonal $\delta^2H_{l\text{-}water}$ signal in *n*-alkanes could be obscured by changes in carbohydrate sourcing (Newberry *et al.*, 2015). We observed that if a signal in leaf δ^2H_{starch} is preserved during its remobilization, it does not necessarily dilute the represented time period. Moreover, there was no period of covariability between δ^2H_{alkane} and δ^2H_{starch} here (Fig. 3b), implying that needle starch reserves were unlikely to be the main reason for the weak hydrological signals in 0N δ^2H_{alkane}.

This is the first study to identify time-integrated climatic or physiological signals in δ^2H_{starch}, which were notably different from those of δ^2H_{WSC} (Fig. 4). For example, 0N δ^2H_{starch} had a relatively strong signal from RH on the day of sampling, like for 0N δ^2H_{WSC}, but the strongest signal in δ^2H_{WSC} was T:A_n, which was not as prominent in δ^2H_{starch}. Contrary to previous findings, here δ^2H_{starch} is not necessarily lower than δ^2H in sugars, in leaves of a C_3 species (Fig. 2a; Schleucher *et al.*, 1999; Schuler *et al.*, 2022; Lehmann *et al.*, 2024b). For example, in 1N δ^2H_{starch} was *c.* 18‰ higher than δ^2H_{WSC} on the same sampling dates. This is likely attributed to seasonal variations *in situ*, since we are the first to measure seasonal δ^2H_{starch} in a natural forest. When δ^2H_{starch} was lower than δ^2H_{WSC}, it can be explained by the ^2H depletion of starch during its synthesis, by the reaction catalyzed by chloroplast phosphoglucose isomerase (EC 5.3.1.9; Schleucher *et al.*, 1999). Lehmann *et al.* (2024b) observed that root δ^2H_{starch} was higher than δ^2H_{WSC}, and this could have been from H isotope exchange between water and intermediates of starch, or by additional sources of isotope fractionation during the metabolic pathway toward starch synthesis in roots. We could extend this to δ^2H_{starch} here, if there were substantial enough intermediaries during its synthesis. Following on, the steep decrease in δ^2H_{starch} at the start of 0N sampling could result from a shift from heterotrophy to autotrophy, as observed in new needle growth of *Pinus pisaster* by Desalme *et al.* (2017). On the sampling dates following the steep δ^2H_{starch} decrease, δ^2H_{starch}

© 2025 The Author(s).
New Phytologist © 2025 New Phytologist Foundation.

did not have a noticeably different trend from δ^2H_{WSC} (Fig. 2b). Nonetheless, the overall differences in δ^2H_{starch} and δ^2H_{WSC} were enough to lead to unique physiological and environmental signals in δ^2H_{starch}, which were different from those for δ^2H_{WSC}. The unique signals in δ^2H_{starch} could obscure the signal in δ^2H_{WSC}, in addition to isotope fractionation by starch remobilization.

The necessity of time scales for interpreting δ^2H bioindicators

It has been previously shown that $\delta^2H_{l\text{-}water}$ heterogeneity is related to δ^2H_{alkane} heterogeneity within a leaf (Zhu *et al.*, 2020; Liu *et al.*, 2021) and that photosynthetic water is likely more exposed to evaporative enrichment (Baca Cabrera *et al.*, 2023). In our study, such heterogeneity also includes the effects of leaf water compartmentation between the chloroplast and cytosol (Baca Cabrera *et al.*, 2023). Our results suggest that needle water heterogeneity does not substantially affect the relationship between δ^2H_{alkane} and bulk $\delta^2H_{n\text{-}water}$ over a timescale of multiple weeks (Fig. 6). This could be due to increased δ^2H_{source} variability over multiple weeks counteracting the role of leaf water heterogeneity (Fig. 3a). For 1N δ^2H_{WSC}, leaf water heterogeneity became more relevant because δ^2H_{WSC} was more strongly related to $\Delta^2H_{n\text{-}water}$ than to $\delta^2H_{n\text{-}water}$ (Fig. 4). This could be because the shorter time integration for δ^2H_{WSC} did not allow δ^2H_{source} to vary enough to be more influential than within-needle isotope heterogeneity. Therefore, while our results are based on moderately performing model gap filling for $\delta^2H_{n\text{-}water}$ and $\Delta^2H_{n\text{-}water}$ (Figs 3a, S5; Table S1), they build on existing evidence (Zhu *et al.*, 2020; Baca Cabrera *et al.*, 2023), suggesting that it is worthwhile to further explore $\delta^2H_{n\text{-}water}$ heterogeneity effects on the prevailing information stored in δ^2H of leaf carbohydrates and thus tree rings. Overall, its different roles to δ^2H_{alkane} and δ^2H_{WSC} suggest that the integration time has the potential to affect not only the period that δ^2H represents but also the factors most influential to δ^2H.

Conclusion

By investigating δ^2H_{alkane}, δ^2H_{WSC} and δ^2H_{starch} in a natural forest, this study has bridged the understanding between leaf-level biosynthetic ^2H-fractionation, and paleoclimatic reconstructions. We have demonstrated that it is critical to use time-integrated analyses when exploring physiological and environmental signals in organic compound δ^2H at the leaf level, especially for *n*-alkanes. Our results indicate that the prevailing physiological signal in leaf sugars could be a mixed signal from different needle ages or seasonal stages, with potential interference from remobilization of δ^2H_{source}- or g_s-signals in δ^2H_{starch}. Thus, it is important to investigate the prevailing information transported by δ^2H in sugars to the phloem. Finally, we demonstrate that *de novo* mature needle δ^2H_{alkane} synthesis in the field is substantial enough to establish a weak relationship with processes correlated with hydrological factors (e.g. RH, δ^2H_{source} and $\delta^2H_{n\text{-}water}$), making it potentially more reliable than 0N δ^2H_{alkane}, which is exposed to more variable biosynthetic isotope fractionation. This finding is promising for paleoclimatic reconstructions, because δ^2H_{alkane} delivered in fallen leaves could possess an integrated palaeohydrological signal from the leaf lifespan. However, we still lack information, to which extent fallen and living leaves contribute to the soil δ^2H_{alkane} reservoir, a topic that should be targeted in future studies.

Acknowledgements

Many thanks to Manuela Oettli and Oliver Rehmann for technical support with extraction and δ^2H analysis of carbohydrates (WSL); Pasi Kolari for sharing the leaf cuvette gas exchange data; Kei Yoshimura for sharing the IsoGSM data; Fanny Petibon and Nicholas Ofiti for their advice with laboratory work. The authors thank the SMEAR staff and the ICOS staff for providing meteorological and gas-exchange data from Hyytiälä Forest Station, Finland. Thank you to two anonymous reviewers for their constructive comments, which greatly benefited the manuscript. This study was funded by the Research Council of Finland (#341984), the Kone Foundation (#202006108), the Swiss National Science Foundation (#204051) and the European Research Council (ERC, #755865). The Research Council of Finland is further acknowledged by KTR-G (#343059) and PSA (#345510 and #358647). MML acknowledges funding by the Swiss National Science Foundation (#179978, #213367).

Competing interests

None declared.

Author contributions

CA, KTR-G, GLBW, MML and MS were involved in conceptualization. YT, PPS-A, KTR-G and ES were involved in fieldwork. CA, GLBW, TCS, MML, MS and YT were involved in laboratory work. CA, GLBW, KTR-G, ES, MML, MS and YT were involved in data quality control. CA was involved in visualization, and modeling and statistical analysis. CA, YT and TCS were involved in writing – original draft. KTR-G, GLBW, MML, YT, TCS, MS, ES, PPS-A and CA were involved in writing – review and editing. KTR-G was involved in supervision. CA, KTR-G, GLBW, MML and MS were involved in funding acquisition.

ORCID

Charlotte Angove https://orcid.org/0000-0003-2622-2667
Marco M. Lehmann https://orcid.org/0000-0003-2962-3351
Katja T. Rinne-Garmston https://orcid.org/0000-0001-9793-2549
Elina Sahlstedt https://orcid.org/0000-0001-8612-6007
Matthias Saurer https://orcid.org/0000-0002-3954-3534
Pauliina P. Schiestl-Aalto https://orcid.org/0000-0003-1369-1923
Tatjana C. Speckert https://orcid.org/0000-0003-3619-0347

© 2025 The Author(s).
New Phytologist © 2025 New Phytologist Foundation.

14698137, 0, Downloaded from https://nph.onlinelibrary.wiley.com/doi/10.1111/nph.20448 by Luonnonvarakeskus, Wiley Online Library on [24/02/2025]. See the Terms and Conditions (https://onlinelibrary.wiley.com/terms-and-conditions) on Wiley Online Library for rules of use; OA articles are governed by the applicable Creative Commons License

Yu Tang https://orcid.org/0000-0002-2851-4762
Guido L. B. Wiesenberg https://orcid.org/0000-0003-2738-5775

Data availability

The novel data that support the findings of this study are available on Dryad doi: 10.5061/dryad.xpnvx0krq. The open-access data from SMEAR and ICOS are accessible via their data portals; 'https://smear.avaa.csc.fi/download' and 'https://data.icos-cp.eu/portal/', respectively.

References

Aalto J, Aalto P, Keronen P, Rantala P, Taipale R, Kajos M, Patokoski J, Rinne J, Ruuskanen T, Leskinen M *et al.* 2023. *SMEAR II Hyytiälä forest meteorology, greenhouse gases, air quality and soil* [Data set]. [WWW document] URL https://etsin.fairdata.fi/dataset/eba017b1-2c68-4874-8a45-5ee28531314f [accessed 14 November 2024].

Aalto J, Kolari P, Hari P, Kerminen VM, Schiestl-Aalto P, Aaltonen H, Levula J, Siivola E, Kulmala M, Bäck J. 2014. New foliage growth is a significant, unaccounted source for volatiles in boreal evergreen forests. *Biogeosciences* **11**: 1331–1344.

Abrahim A, Cannavan A, Kelly SD. 2020. Stable isotope analysis of non-exchangeable hydrogen in carbohydrates derivatised with N-methyl-bis-trifluoroacetamide by gas chromatography – chromium silver reduction/high temperature conversion-isotope ratio mass spectrometry (GC-CrAg/HTC-IRMS). *Food Chemistry* **318**: 126413.

Angove C, Lehmann MM, Saurer M, Tang Y, Kilpeläinen P, Kahmen A, Schiestl-Aalto PP, Tikkasalo OP, Bäck JK, Rinne-Garmston KT. 2023. Unsaturated intercellular vapor pressure is relevant for leaf water heavy isotope enrichment. *bioRxiv*. doi: 10.1101/2023.09.12.557463.

Augusti A, Betson TR, Schleucher J. 2006. Hydrogen exchange during cellulose synthesis distinguishes climatic and biochemical isotope fractionations in tree rings. *New Phytologist* **172**: 490–499.

Baan J, Holloway-Phillips M, Nelson DB, Kahmen A. 2023a. The metabolic sensitivity of hydrogen isotope fractionation differs between plant compounds. *Phytochemistry* **207**: 113563.

Baan J, Holloway-Phillips M, Nelson DB, Kahmen A. 2023b. Species and biosynthetic effects cause uncorrelated variation in oxygen and hydrogen isotope compositions of plant organic compounds. *Geochimica et Cosmochimica Acta* **352**: 1–13.

Baca Cabrera JC, Hirl RT, Zhu J, Schäufele R, Ogée J, Schnyder H. 2023. ^{18}O enrichment of sucrose and photosynthetic and nonphotosynthetic leaf water in a C_3 grass – atmospheric drivers and physiological relations. *Plant, Cell & Environment* **46**: 2628–2648.

Barbour MM, Farquhar GD. 2000. Relative humidity- and ABA-induced variation in carbon and oxygen isotope ratios of cotton leaves. *Plant, Cell & Environment* **23**: 473–485.

Barbour MM, White MA, Liu L. 2024. $H_2{}^{18}O$ vapour labelling reveals evidence of radial Péclet effects, but in not all leaves. *New Phytologist* **244**: 1263–1274.

Barnard RL, Salmon Y, Kodama N, Sörgel K, Holst J, Rennenberg H, Gessler A, Buchmann N. 2007. Evaporative enrichment and time lags between $\delta^{18}O$ of leaf water and organic pools in a pine stand. *Plant, Cell & Environment* **30**: 539–550.

von Caemmerer S, Farquhar GD. 1981. Some relationships between the biochemistry of photosynthesis and the gas exchange of leaves. *Planta* **153**: 376–387.

Cernusak LA, Barbeta A, Bush RT, Eichstaedt R, Ferrio JP, Flanagan LB, Gessler A, Martín-Gómez P, Hirl RT, Kahmen A *et al.* 2022. Do ^2H and ^{18}O in leaf water reflect environmental drivers differently? *New Phytologist* **235**: 41–51.

Cernusak LA, Barbour MM, Arndt SK, Cheesman AW, English NB, Feild TS, Helliker BR, Holloway-Phillips MM, Holtum JA, Kahmen A *et al.* 2016. Stable isotopes in leaf water of terrestrial plants. *Plant, Cell & Environment* **39**: 1087–1102.

Cernusak LA, Farquhar GD, Wong SC, Stuart-Williams H. 2004. Measurement and interpretation of the oxygen isotope composition of carbon dioxide respired by leaves in the dark. *Plant Physiology* **136**: 3350–3363.

Cernusak LA, Wong SC, Stuart-Williams H, Márquez DA, Pontarin N, Farquhar GD. 2024. Unsaturation in the air spaces of leaves and its implications. *Plant, Cell & Environment* **47**: 3685–3698.

Conte MH, Weber JC. 2002. Long-range atmospheric transport of terrestrial biomarkers to the western North Atlantic. *Global Biogeochemical Cycles* **16**: 89-1–89-17.

Cormier MA, Werner RA, Sauer PE, Gröcke DR, Leuenberger MC, Wieloch T, Schleucher J, Kahmen A. 2018. ^2H-fractionations during the biosynthesis of carbohydrates and lipids imprint a metabolic signal on the δ^2H values of plant organic compounds. *New Phytologist* **218**: 479–491.

Dawson D, Grice K, Wang SX, Alexander R, Radke J. 2004. Stable hydrogen isotopic composition of hydrocarbons in torbanites (Late Carboniferous to Late Permian) deposited under various climatic conditions. *Organic Geochemistry* **35**: 189–197.

Desalme D, Priault P, Gérant D, Dannoura M, Maillard P, Plain C, Epron D. 2017. Seasonal variations drive short-term dynamics and partitioning of recently assimilated carbon in the foliage of adult beech and pine. *New Phytologist* **213**: 140–153.

Farquhar GD, Gan KS. 2003. On the progressive enrichment of the oxygen isotopic composition of water along a leaf. *Plant, Cell & Environment* **26**: 1579–1597.

Fernandez O, Ishihara H, George GM, Mengin V, Flis A, Sumner D, Arrivault S, Feil R, Lunn JE, Zeeman SC *et al.* 2017. Leaf starch turnover occurs in long days and in falling light at the end of the day. *Plant Physiology* **174**: 2199–2212.

Freimuth EJ, Diefendorf AF, Lowell TV. 2017. Hydrogen isotopes of n-alkanes and n-alkanoic acids as tracers of precipitation in a temperate forest and implications for paleorecords. *Geochimica et Cosmochimica Acta* **206**: 166–183.

Gaastra P. 1959. *Photosynthesis of crop plants as influenced by light, carbon dioxide, temperature and stomatal diffusion resistance*. PhD thesis, Mededelingen van de Landbouwhogeschool te Wageningen, Nederland.

Gan SC, Wong SC, Yong JW, Farquhar GD. 2002. ^{18}O spatial patterns of vein xylem water, leaf water, and dry matter in cotton leaves. *Plant Physiology* **130**: 1008–1021.

Geigenberger P, Stitt M. 1991. A "futile" cycle of sucrose synthesis and degradation is involved in regulating partitioning between sucrose, starch and respiration in cotyledons of germinating *Ricinus communis* L. seedlings when phloem transport is inhibited. *Planta* **185**: 81–90.

Gessler A, Brandes E, Buchmann N, Helle G, Rennenberg H, Barnard RL. 2009. Tracing carbon and oxygen isotope signals from newly assimilated sugars in the leaves to the tree-ring archive. *Plant, Cell & Environment* **32**: 780–795.

Gessler A, Brandes E, Keitel C, Boda S, Kayler ZE, Granier A, Barbour M, Farquhar GD, Treydte K. 2013. The oxygen isotope enrichment of leaf-exported assimilates – does it always reflect lamina leaf water enrichment? *New Phytologist* **200**: 144–157.

Hepp J, Mayr C, Rozanski K, Schäfer IK, Tuthorn M, Glaser B, Juchelka D, Stichler W, Zech R, Zech M. 2021. Validation of a coupled $\delta^2H_{n\text{-alkane}}$-$\delta^{18}O_{sugar}$ paleohygrometer approach based on a climate chamber experiment. *Biogeosciences* **18**: 5363–5380.

Holloway-Phillips M, Baan J, Nelson DB, Lehmann MM, Tcherkez G, Kahmen A. 2022. Species variation in the hydrogen isotope composition of leaf cellulose is mostly driven by isotopic variation in leaf sucrose. *Plant, Cell & Environment* **45**: 2636–2651.

Jetter R, Schäffer S. 2001. Chemical composition of the *Prunus laurocerasus* leaf surface. Dynamic changes of the epicuticular wax film during leaf development. *Plant Physiology* **126**: 1725–1737.

Jetter R, Schäffer S, Riederer M. 2000. Leaf cuticular waxes are arranged in chemically and mechanically distinct layers: evidence from *Prunus laurocerasus* L. *Plant, Cell & Environment* **23**: 619–628.

Jupyter. 2022. *Jupyter notebook: the classic notebook interface*. Project Jupyter.

Kahmen A, Dawson TE, Vieth A, Sachse D. 2011. Leaf wax n-alkane δD values are determined early in the ontogeny of *Populus trichocarpa* leaves when grown

© 2025 The Author(s).
New Phytologist © 2025 New Phytologist Foundation.

14698137, 0, Downloaded from https://nph.onlinelibrary.wiley.com/doi/10.1111/nph.20448 by Luonnonvarakeskus, Wiley Online Library on [24/02/2025]. See the Terms and Conditions (https://onlinelibrary.wiley.com/terms-and-conditions) on Wiley Online Library for rules of use; OA articles are governed by the applicable Creative Commons License

under controlled environmental conditions. *Plant, Cell & Environment* **34**: 1639–1651.

Kahmen A, Schefuß E, Sachse D. 2013. Leaf water deuterium enrichment shapes leaf wax n-alkane δd values of angiosperm plants I: Experimental evidence and mechanistic insights. *Geochimica et Cosmochimica Acta* **111**: 39–49.

Kolari P, Aalto J, Levula J, Kulmala L, Ilvesniemi H, Pumpanen J. 2022. *Hyytiälä SMEAR II site characteristics* [Data set]. [WWW document] URL https://dspace.uef.fi/handle/123456789/26786 [accessed 16 February 2023].

Kolari P, Bäck J, Taipale R, Ruuskanen TM, Kajos MK, Rinne J, Kulmala M, Hari P. 2012. Evaluation of accuracy in measurements of VOC emissions with dynamic chamber system. *Atmospheric Environment* **62**: 344–351.

Lehmann MM, Diao H, Ouyang S, Gessler A. 2024a. Different responses of oxygen and hydrogen isotopes in leaf and tree-ring organic matter to lethal soil drought. *Tree Physiology* **44**: tpae043.

Lehmann MM, Ghiasi S, George GM, Cormier MA, Gessler A, Saurer M, Werner RA. 2019. Influence of starch deficiency on photosynthetic and post-photosynthetic carbon isotope fractionations. *Journal of Experimental Botany* **70**: 1829–1841.

Lehmann MM, Schuler P, Cormier MA, Allen ST, Leuenberger M, Voelker S. 2022. The stable hydrogen isotopic signature: from source water to tree rings. In: Siegwolf RTW, Brooks JR, Roden J, Saurer M, eds. *Stable isotopes in tree rings: inferring physiological, climatic and environmental responses*. Cham, Switzerland: Springer, 331–359.

Lehmann MM, Schuler P, Werner RA, Saurer M, Wiesenberg GL, Cormier MA. 2024b. Biochemical and biophysical drivers of the hydrogen isotopic composition of carbohydrates and acetogenic lipids. *Science Advances* **10**: eadl3591.

Lehmann MM, Vitali V, Schuler P, Leuenberger M, Saurer M. 2021. More than climate: hydrogen isotope ratios in tree rings as novel plant physiological indicator for stress conditions. *Dendrochronologia* **65**: 125788.

Leppä K, Tang Y, Ogée J, Launiainen S, Kahmen A, Kolari P, Sahlstedt E, Saurer M, Schiestl-Aalto P, Rinne-Garmston KT. 2022. Explicitly accounting for needle sugar pool size crucial for predicting intra-seasonal dynamics of needle carbohydrates $\delta^{18}O$ and $\delta^{13}C$. *New Phytologist* **236**: 2044–2060.

Liu J, An Z, Lin G. 2021. Intra-leaf heterogeneities of hydrogen isotope compositions in leaf water and leaf wax of monocots and dicots. *Science of the Total Environment* **770**: 145258.

Liu J, Zhao J, He D, Huang X, Jiang C, Yan H, Lin G, An Z. 2022. Effects of plant types on terrestrial leaf wax long-chain n-alkane biomarkers: implications and paleoapplications. *Earth-Science Reviews* **235**: 104248.

Luo Y-H, Sternberg L. 1992. Spatial D/H heterogeneity of leaf water. *Plant Physiology* **99**: 348–350.

Maloney AE, Kopf SH, Zhang Z, McFarlin J, Nelson DB, Masterson AL, Zhang X. 2024. Large enrichments in fatty acid 2H/1H ratios distinguish respiration from aerobic fermentation in yeast Saccharomyces cerevisiae. *Proceedings of the National Academy of Sciences, USA* **121**: e2310771121.

Mammarella I, Aalto J, Back J, Kolari P, Laakso H, Levula J, Matilainen T, Pihlatie M, Pumpanen J, Ryhti K *et al.* 2024. *ETC L2 Fluxes, Hyytiala, 2017-12-31–2024-10-20, ICOS RI* [Data set]. [WWW document] URL https://hdl.handle.net/11676/8MwqJXArIZH3AtxKArglmMOV [accessed 16 February 2023].

McInerney FA, Helliker BR, Freeman KH. 2011. Hydrogen isotope ratios of leaf wax n-alkanes in grasses are insensitive to transpiration. *Geochimica et Cosmochimica Acta* **75**: 541–554.

Newberry SL, Kahmen A, Dennis P, Grant A. 2015. n-Alkane biosynthetic hydrogen isotope fractionation is not constant throughout the growing season in the riparian tree *Salix viminalis*. *Geochimica et Cosmochimica Acta* **165**: 75–85.

Ofiti NOE, Altermatt M, Petibon F, Warren JM, Malhotra A, Hanson PJ, Wiesenberg GL. 2023. Warming and elevated CO_2 induced shifts in carbon partitioning and lipid composition within an ombrotrophic bog plant community. *Environmental and Experimental Botany* **206**: 105182.

Ogée J, Barbour MM, Wingate L, Bert D, Bosc A, Stievenard M, Lambrot C, Pierre M, Bariac T, Loustau D *et al.* 2009. A single-substrate model to interpret intra-annual stable isotope signals in tree-ring cellulose. *Plant, Cell & Environment* **32**: 1071–1090.

Pérez-de-Lis G, Rathgeber C, Fernández de Uña L, Ponton S. 2022. Cutting tree rings into time slices: how intra-annual dynamics of wood formation help decipher the space-for-time conversion. *New Phytologist* **233**: 1520–1534.

R Core Team. 2022. *R: A language and environment for statistical computing*. Vienna, Austria: R Foundation for Statistical Computing.

Rinne KT, Saurer M, Streit K, Siegwolf RT. 2012. Evaluation of a liquid chromatography method for compound-specific $\delta^{13}C$ analysis of plant carbohydrates in alkaline media. *Rapid Communications in Mass Spectrometry* **26**: 2173–2185.

van Rossum G, Drake FL. 2009. *Python 3 reference manual*. Scotts Valley, CA, USA: CreateSpace.

Sachse D, Dawson TE, Kahmen A. 2015. Seasonal variation of leaf wax n-alkane production and δ2H values from the evergreen oak tree, *Quercus agrifolia*. *Isotopes in Environmental and Health Studies* **51**: 124–142.

Sachse D, Radke J, Gleixner G. 2006. δD values of individual n-alkanes from terrestrial plants along a climatic gradient – implications for the sedimentary biomarker record. *Organic Geochemistry* **37**: 469–483.

Schefuß E, Schouten S, Schneider R. 2005. Climatic controls on central African hydrology during the past 20,000 years. *Nature* **437**: 1003–1006.

Schleucher J, Vanderveer P, Markley JL, Sharkey TD. 1999. Intramolecular deuterium distributions reveal disequilibrium of chloroplast phosphoglucose isomerase. *Plant, Cell & Environment* **22**: 525–533.

Schuler P, Cormier MA, Werner RA, Buchmann N, Gessler A, Vitali V, Saurer M, Lehmann MM. 2022. A high-temperature water vapor equilibration method to determine non-exchangeable hydrogen isotope ratios of sugar, starch and cellulose. *Plant, Cell & Environment* **45**: 12–22.

Sessions AL, Burgoyne TW, Schimmelmann A, Hayes JM. 1999. Fractionation of hydrogen isotopes in lipid biosynthesis. *Organic Geochemistry* **30**: 1193–1200.

Song X, Barbour MM, Farquhar GD, Vann DR, Helliker BR. 2013. Transpiration rate relates to within- and across-species variations in effective path length in a leaf water model of oxygen isotope enrichment. *Plant, Cell & Environment* **36**: 1338–1351.

Speckert TC, Petibon F, Wiesenberg GLB. 2023. Late-season biosynthesis of leaf fatty acids and n-alkanes of a mature beech (*Fagus sylvatica*) tree traced via $^{13}CO_2$ pulse-chase labelling and compound-specific isotope analysis. *Frontiers in Plant Science* **13**: 1029026.

Srivastava K, Wiesenberg GLB. 2018. Severe drought-influenced composition and $\delta^{13}C$ of plant and soil n-alkanes in model temperate grassland and heathland ecosystems. *Organic Geochemistry* **116**: 77–89.

Tang Y, Schiestl-Aalto P, Lehmann MM, Saurer M, Sahlstedt E, Kolari P, Leppä K, Bäck J, Rinne-Garmston KT. 2023. Estimating intra-seasonal photosynthetic discrimination and water use efficiency using $\delta^{13}C$ of leaf sucrose in Scots pine. *Journal of Experimental Botany* **74**: 321–335.

Tang Y, Schiestl-Aalto P, Saurer M, Sahlstedt E, Kulmala L, Kolari P, Ryhti K, Salmon Y, Jyske T, Ding Y *et al.* 2022. Tree organ growth and carbon allocation dynamics impact the magnitude and $\delta^{13}C$ signal of stem and soil CO_2 fluxes. *Tree Physiology* **42**: 2404–2418.

Tang Y, Sahlstedt E, Rissanen K, Bäck J, Schiestl-Aalto P, Angove C, Richter A, Saurer M, Aalto J, Dukat P *et al.* 2024. Resin acid $\delta^{13}C$ and $\delta^{18}O$ as indicators of intra-seasonal physiological and environmental variability. *Plant, Cell & Environment* **47**: 5411–5423.

Thomas CL, Jansen B, van Loon EE, Wiesenberg GL. 2021. Transformation of n-alkanes from plant to soil: a review. *Soil* **7**: 785–809.

Tipple BJ, Berke MA, Hambach B, Roden JS, Ehleringer JR. 2015. Predicting leaf wax n-alkane $^{2}H/^{1}H$ ratios: controlled water source and humidity experiments with hydroponically grown trees confirm predictions of Craig–Gordon model. *Plant, Cell & Environment* **38**: 1035–1047.

Tipple BJ, Ehleringer JR. 2018. Distinctions in heterotrophic and autotrophic-based metabolism as recorded in the hydrogen and carbon isotope ratios of normal alkanes. *Oecologia* **187**: 1053–1075.

Vitali V, Martínez-Sancho E, Treydte K, Andreu-Hayles L, Dorado-Liñán I, Gutierrez E, Helle G, Leuenberger M, Loader NJ, Rinne-Garmston KT *et al.* 2022. The unknown third – hydrogen isotopes in tree-ring cellulose across Europe. *Science of the Total Environment* **813**: 152281.

Vitali V, Peters RL, Lehmann MM, Leuenberger M, Treydte K, Büntgen U, Schuler P, Saurer M. 2023. Tree-ring isotopes from the Swiss Alps reveal non-

© 2025 The Author(s).
New Phytologist © 2025 New Phytologist Foundation.

14698137, 0, Downloaded from https://nph.onlinelibrary.wiley.com/doi/10.1111/nph.20448 by Luonnonvarakeskus, Wiley Online Library on [24/02/2025]. See the Terms and Conditions (https://onlinelibrary.wiley.com/terms-and-conditions) on Wiley Online Library for rules of use; OA articles are governed by the applicable Creative Commons License

climatic fingerprints of cyclic insect population outbreaks over the past 700 years. *Tree Physiology* **43**: 706–721.

Wanek W, Heintel S, Richter A. 2001. Preparation of starch and other carbon fractions from higher plant leaves for stable carbon isotope analysis. *Rapid Communications in Mass Spectrometry* **15**: 1136–1140.

Weise SE, van Wijk KJ, Sharkey TD. 2011. The role of transitory starch in C_3, CAM, and C_4 metabolism and opportunities for engineering leaf starch accumulation. *Journal of Experimental Botany* **62**: 3109–3118.

Wieloch T, Grabner M, Augusti A, Serk H, Ehlers I, Yu J, Schleucher J. 2022. Metabolism is a major driver of hydrogen isotope fractionation recorded in tree-ring glucose of *Pinus nigra*. *New Phytologist* **234**: 449–461.

Wieloch T, Holloway-Phillips M, Yu J, Niittylä T. 2024. New insights into the mechanisms of plant isotope fractionation from combined analysis of intramolecular ^{13}C and deuterium abundances in *Pinus nigra* tree-ring glucose. *New Phytologist* **245**: 1000–1017.

Wieloch T, Werner RA, Schleucher J. 2021. Carbon flux around leaf-cytosolic glyceraldehyde-3-phosphate dehydrogenase introduces a ^{13}C signal in plant glucose. *Journal of Experimental Botany* **72**: 7136–7144.

Wiesenberg GLB, Gocke MI. 2015. Analysis of lipids and polycyclic aromatic hydrocarbons as indicators of past and present (micro)biological activity. In: McGenity T, Timmis K, Nogales B, eds. *Hydrocarbon and lipid microbiology protocols*. Berlin, Heidelberg, Germany: Springer, 61–91.

Wijker RS, Sessions AL, Fuhrer T, Phan M. 2019. $^2H/^1H$ variation in microbial lipids is controlled by NADPH metabolism. *Proceedings of the National Academy of Sciences, USA* **116**: 12173–12182.

Wong SC, Cowan IR, Farquhar GD. 1979. Stomatal conductance correlates with photosynthetic capacity. *Nature* **282**: 424–426.

Yakir D. 1992. Variations in the natural abundance of oxygen-18 and deuterium in plant carbohydrates. *Plant, Cell & Environment* **15**: 1005–1020.

Yan CF, Han SJ, Zhou YM, Wang CG, Dai GH, Xiao WF, Li MH. 2012. Needle-age related variability in nitrogen, mobile carbohydrates, and $\delta^{13}C$ within pinus koraiensis tree crowns. *PLoS ONE* **7**: e35076.

Yoshimura K, Frankenberg C, Lee J, Kanamitsu M, Worden J, Röckmann T. 2011. Comparison of an isotopic atmospheric general circulation model with new quasi-global satellite measurements of water vapor isotopologues. *Journal of Geophysical Research: Atmospheres* **116**: 1–15.

Yoshimura K, Kanamitsu M, Noone D, Oki T. 2008. Historical isotope simulation using Reanalysis atmospheric data. *Journal of Geophysical Research: Atmospheres* **113**: 1–15.

Zech M, Zech R, Rozanski K, Gleixner G, Zech W. 2015. Do n-alkane biomarkers in soils/sediments reflect the δ2H isotopic composition of precipitation? A case study from Mt. Kilimanjaro and implications for paleoaltimetry and paleoclimate research. *Isotopes in Environmental and Health Studies* **51**: 508–524.

Zhou Y, Grice K, Stuart-Williams H, Hocart CH, Gessler A, Farquhar GD. 2016. Hydrogen isotopic differences between C_3 and C_4 land plant lipids: consequences of compartmentation in C_4 photosynthetic chemistry and C_3 photorespiration. *Plant, Cell & Environment* **39**: 2676–2690.

Zhu Z, Xu B, Günther F, Gleixner G. 2020. Leaf transition from heterotrophy to autotrophy is recorded in the intraleaf C, H and O isotope patterns of leaf organic matter. *Rapid Communications in Mass Spectrometry* **34**: e8840.

Supporting Information

Additional Supporting Information may be found online in the Supporting Information section at the end of the article.

Fig. S1 Transpiration rate measured from two gas cuvette exchange systems with gap filling by model replication.

Fig. S2 Successfully replicated source $\delta^{18}O$ predictions from Leppä *et al.* (2022).

Fig. S3 Relationships between measured δ^2H and $\delta^{18}O$ in source water and water vapor.

Fig. S4 Relationships between oxygen-18 ($\delta^{18}O$, ‰) and deuterium (δ^2H, ‰) for modeled and measured soil water and twig water.

Fig. S5 Quality of different isotope modeling for leaf water heavy isotope values and enrichment when measured δ^2H data for source water and water vapor are missing.

Methods S1 Description for extraction of water-soluble carbohydrates and starch.

Methods S2 Description of isotope modeling to implement in time-integrated analyses.

Table S1 Regression fits showing the performance of different isotope modeling for leaf water heavy isotope values and enrichment when measured δ^2H data for source water and water vapor are missing.

Table S2 Mean biosynthetic hydrogen isotope fractionation between modeled leaf water and measured leaf organic compounds.

Please note: Wiley is not responsible for the content or functionality of any Supporting Information supplied by the authors. Any queries (other than missing material) should be directed to the *New Phytologist* Central Office.

Disclaimer: The New Phytologist Foundation remains neutral with regard to jurisdictional claims in maps and in any institutional affiliations.

© 2025 The Author(s).
New Phytologist © 2025 New Phytologist Foundation.

14698137, 0, Downloaded from https://nph.onlinelibrary.wiley.com/doi/10.1111/nph.20448 by Luonnonvarakeskus, Wiley Online Library on [24/02/2025]. See the Terms and Conditions (https://onlinelibrary.wiley.com/terms-and-conditions) on Wiley Online Library for rules of use; OA articles are governed by the applicable Creative Commons License